
Efficient Cross-Domain Offline Reinforcement Learning with Dynamics- and Value-Aligned Data Filtering

Zhongjian Qiao¹ Rui Yang² Jiafei Lyu³ Chenjia Bai⁴ Xiu Li⁵ Siyang Gao¹ Shuang Qiu^{†1}

Abstract

Cross-domain offline reinforcement learning (RL) aims to train a well-performing agent in the target environment, leveraging both a limited target domain dataset and a source domain dataset with (possibly) sufficient data coverage. Due to the underlying dynamics misalignment between source and target domains, naively merging the two datasets may incur inferior performance. Recent advances address this issue by selectively leveraging source domain samples whose dynamics align well with the target domain. However, our work demonstrates that dynamics alignment alone is insufficient, by examining the limitations of prior frameworks and deriving a new target domain sub-optimality bound for the policy learned on the source domain. More importantly, our theory underscores an additional need for *value alignment*, i.e., selecting high-quality, high-value samples from the source domain, a critical dimension overlooked by existing works. Motivated by such theoretical insight, we propose **D**ynamics- and **V**alue-aligned **D**ata **F**iltering (DVDF) method, a novel unified cross-domain RL framework that selectively incorporates source domain samples exhibiting strong alignment in *both dynamics and values*. We empirically study a range of dynamics shift scenarios, including kinematic and morphology shifts, and evaluate DVDF on various tasks and datasets, even in the challenging setting where the target domain dataset contains an extremely limited amount of data. Extensive experiments demonstrate that DVDF consistently outperforms strong baselines with significant improvements. Our code is available at <https://github.com/zq2r/DVDF.git>.

¹City University of Hong Kong ²University of Illinois Urbana-Champaign ³Tencent ⁴Institute of Artificial Intelligence, China Telecom (TeleAI) ⁵Tsinghua University. [†]Corresponding Author. Correspondence to: Shuang Qiu <shuangqiu@cityu.edu.hk>.

1. Introduction

Reinforcement learning (RL) (Sutton & Barto, 1999) has seen remarkable progress in fields like video games (Ye et al., 2020; Mnih et al., 2013) and robotics (Kober et al., 2013; Kormushev et al., 2013). However, the frequent interactions required for online RL can be expensive or risky in real-world applications. Offline RL (Levine et al., 2020; Prudencio et al., 2023) addresses this by learning from pre-collected datasets, eliminating the need for online interaction. Yet, its performance is often constrained by the limited size of target datasets, as extensive data collection remains costly. To overcome this, cross-domain offline RL (Wen et al., 2024; Liu et al., 2022; 2024a) leverages additional data (called source domain) collected from environments related to but distinct from the target one for policy learning.

Although the idea of leveraging additional source domain data to benefit target policy learning is promising, the key challenge lies in that the source and target environments may differ in transition dynamics, and simply merging the source and target data for training could degrade the performance (Wen et al., 2024; Liu et al., 2024a) due to the out-of-distribution (OOD) transition dynamics issue (Liu et al., 2024a). Previous solutions for this issue include training a domain classifier for reward augmentation (Liu et al., 2022; Eysenbach et al., 2020), using supported value optimization and conservative regularization to mitigate overestimation (Liu et al., 2024a), etc. Recent advances (Xu et al., 2024; Wen et al., 2024; Lyu et al., 2025) introduce dynamics-aware data filtering, where source domain samples are selectively shared based on their alignment with the target dynamics to enhance policy learning. For example, and IGDF (Wen et al., 2024) leverages contrastive representation for data filtering, OTDF (Lyu et al., 2025) selects source domain data based on optimal transport. Despite methodological differences, these studies share a common idea: *source domain samples with smaller dynamics misalignment facilitate target policy learning, whereas those with larger misalignment impede it*. However, we argue that this point may not universally hold, as it overlooks the significance of *value alignment*: the selected data should also exhibit high quality other than aligned dynamics. Intuitively, high-quality source samples with moderate dynamics mis-

alignment may contribute more to target policy learning than low-quality samples that are well aligned in dynamics. Consider the case where the source domain dataset consists of non-expert low-quality samples with minor dynamics misalignment and expert samples with larger dynamics misalignment. Methods based on dynamics-aware data filtering will only select low-quality samples, although these samples may contribute little to policy learning. Instead, incorporating expert samples (despite larger dynamics misalignment) may yield better performance. Therefore, we raise the question: *Can we devise a cross-domain offline RL method that jointly considers dynamics alignment and value alignment?*

In this paper, we propose a simple yet effective solution for the above question, called **D**ynamics- and **V**alue-aligned **D**ata **F**iltering (DVDF). We start with a motivating example to empirically show that only considering dynamics alignment is not enough for efficient cross-domain offline RL. From a theoretical perspective, we reveal that existing theoretical frameworks that *focus on tightening the performance discrepancy of a given policy between the source and target domain misalign with the learning objective*, and fails to guarantee learning a well-performing target policy. This explains the limitations of the recent methods like IGDF and OTDF. Alternatively, we derive a concrete sub-optimality bound for policies trained on the source domain and evaluated on the target domain, demonstrating that both dynamics and value alignments are essential for cross-domain offline RL. Based on this theoretical insight, we present our method, DVDF, which utilizes an advantage function pre-trained on the source domain to measure the value misalignment and incorporates dynamics-aware data filtering to capture the dynamics misalignment within a unified framework. Then DVDF trades off dynamics and value misalignment and selectively shares source domain samples to train the policy. DVDF can be generally treated as a **plug-in module** and seamlessly integrated with recent methods like IGDF and OTDF. Our contributions can be summarized as follows.

- We examine the limitations of the current theoretical analysis framework for cross-domain offline RL, and theoretically demonstrate that both dynamics alignment and value alignment are essential for cross-domain offline RL, providing new insights for the field.
- Based on the theoretical insight, we propose our method, DVDF, which jointly considers dynamics alignment and value alignment, and selectively shares source domain data for policy learning. DVDF is a plug-in module and can be integrated into other methods like IGDF and OTDF.
- We conduct extensive experiments across various dynamics shift conditions, which demonstrate that DVDF exhibits superior performance on many tasks and datasets compared to strong baselines. We further test DVDF under challenging conditions where the target domain

dataset is extremely limited (Lyu et al., 2024b; 2025), and observe DVDF delivers exceptional performance.

2. Preliminaries

We consider a Markov Decision Process (MDP) (Puterman, 1990) defined by the six-tuple $\mathcal{M} = (\mathcal{S}, \mathcal{A}, P, r, \rho, \gamma)$ where \mathcal{S} is the state space, \mathcal{A} is the action space, $P : \mathcal{S} \times \mathcal{A} \rightarrow \Delta(\mathcal{S})$ is the transition dynamics, $\Delta(\cdot)$ is the probability simplex, $r(s, a) : \mathcal{S} \times \mathcal{A} \rightarrow [-r_{\max}, r_{\max}]$ is the reward function, ρ is the initial state distribution, and γ is the discount factor. RL aims to learn a policy $\pi : \mathcal{S} \rightarrow \Delta(\mathcal{A})$ that maximizes the objective $J_{\mathcal{M}}(\pi) := \mathbb{E}_{\pi} [\sum_{t=0}^{\infty} \gamma^t r(s_t, a_t)]$.

In the cross-domain RL setting, we assume that we have access to a *source domain* $\mathcal{M}_{\text{src}} = (\mathcal{S}, \mathcal{A}, P_{\text{src}}, r, \rho, \gamma)$ and a *target domain* $\mathcal{M}_{\text{tar}} = (\mathcal{S}, \mathcal{A}, P_{\text{tar}}, r, \rho, \gamma)$. The only difference between the two domains is the transition dynamics. In the offline setting, only a target domain dataset $\mathcal{D}_{\text{tar}} = \{(s_i, a_i, r_i, s_{i+1})\}_{i=1}^{N_1}$ and a source domain dataset $\mathcal{D}_{\text{src}} = \{(s_i, a_i, r_i, s_{i+1})\}_{i=1}^{N_2}$ are available, where $N_1 \ll N_2$. The goal of cross-domain offline RL is to leverage \mathcal{D}_{tar} and \mathcal{D}_{src} to improve the performance of the agent in the target domain, where \mathcal{D}_{src} and \mathcal{D}_{tar} denote the datasets collected in the source and target domain, respectively.

3. Motivating Example: Dynamics Alignment Alone Is Insufficient

In this section, we use a simple example to demonstrate our claim: solely considering dynamics alignment is insufficient for efficient cross-domain offline RL.

We consider the following cross-domain RL scenario: the target domain is `hopper-v2` task from MuJoCo (Todorov et al., 2012), and the source domain is `hopper-v2` task with morphology shift (the head size of the robot is increased), called `hopper-morph-v2`. We visualize the morphology of the robots in Figure 1 (a). In the offline setting, we require both source and target domain datasets. For the target domain, we extract a 10% subset from the `hopper-medium-v2` dataset in D4RL (Fu et al., 2020). The source domain comprises a mixture of: (1) 0.5M random-level samples from `hopper-random-v2` dataset, and (2) 0.5M expert-level samples collected by a well-trained SAC (Haarnoja et al., 2018) policy in the `hopper-morph-v2` environment. Given such source and target domain datasets, we implement the original IGDF (Wen et al., 2024) and our proposed DVDF method (based on IGDF) for source data filtering and target policy learning. We set the source data selection ratio to 25% for both DVDF and IGDF.

We visualize the source data filtering results of IGDF and DVDF using t-SNE (Van der Maaten & Hinton, 2008), as

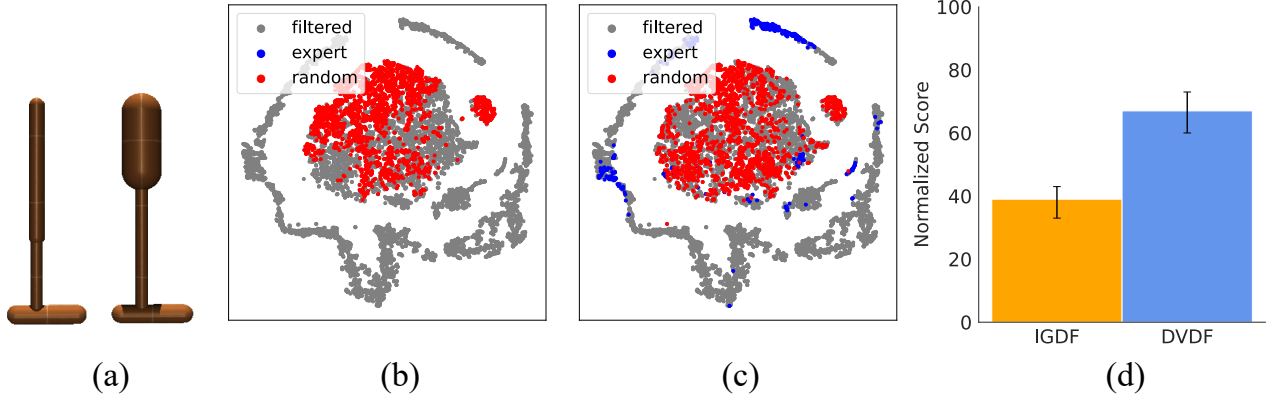


Figure 1. (a) Robot morphology visualization of target domain (left) and source domain (right). (b) Source data filtering visualization of IGDF. (c) Source data filtering visualization of DVDF. (d) Performance comparison between IGDF and DVDF on the target domain.

shown in Figure 1 (b) and (c), respectively. The gray points represent filtered samples, blue points indicate selected expert samples exhibiting dynamics shifts, and red points denote selected random samples without dynamics shifts. The result reveals that IGDF exclusively selects random samples, whereas DVDF incorporates both random and expert samples. We further evaluate the policies trained by each method in the target environment, with the normalized score presented in Figure 1 (d). The results demonstrate that DVDF achieves a significantly higher average score of 67 compared to 39 obtained by IGDF, representing a 71% performance improvement. This substantial improvement demonstrates that the shifted expert data can significantly enhance policy learning, validating our motivation that efficient cross-domain policy learning requires joint consideration of both dynamics and value alignment. More details and results can be found in Appendix D.2.

4. What is Truly Essential for Efficient Cross-Domain Offline RL?

In this section, we provide theoretical insights for our motivation by rethinking and examining the limitations of the current theoretical framework for cross-domain RL. Our analysis reveals a fundamental gap in the existing theoretical foundation, prompting us to answer an important question: *what is truly essential for efficient cross-domain offline RL?*

To answer the above question, we first present the key theoretical framework for recent cross-domain RL methods (Wen et al., 2024; Lyu et al., 2025; Xu et al., 2024; Lyu et al., 2024a) in Lemma 4.1, which mainly relies on establishing a performance difference bound of a given policy between the source and target domain:

Lemma 4.1 (Performance difference bounded by the dynamics misalignment). *Denote the MDP of the source domain and target domain as \mathcal{M}_{src} and \mathcal{M}_{tar} . We have the*

performance difference of a policy π under \mathcal{M}_{src} and \mathcal{M}_{tar} as below,

$$\begin{aligned} & |J_{\mathcal{M}_{\text{tar}}}(\pi) - J_{\mathcal{M}_{\text{src}}}(\pi)| \\ & \leq C_1 \cdot \underbrace{\sup_{s,a} [D_{\text{TV}}(P_{\text{src}}(\cdot|s,a), P_{\text{tar}}(\cdot|s,a))]}_{\text{dynamics misalignment}}, \end{aligned} \quad (1)$$

where $C_1 = \frac{2\gamma\tau_{\max}}{(1-\gamma)^2}$ is a positive constant.

According to Lemma 4.1, the performance difference is bounded by the dynamics misalignment between the source and target domains. Thus, selectively sharing source domain samples with smaller dynamics misalignment can tighten the performance difference, which builds the theoretical foundation for prior studies (Wen et al., 2024; Xu et al., 2024; Lyu et al., 2024a; 2025). However, a critical limitation of this analysis is that **it misaligns with the RL objective**, that is, obtaining a policy π to maximize $J_{\mathcal{M}_{\text{tar}}}(\pi)$. Therefore, tightening such a performance difference bound does not necessarily lead to a well-performing policy in the target domain. Instead, it is more reasonable to narrow the sub-optimality gap of a policy π trained on the source domain and evaluated on the target domain. Specifically, we denote the optimal policy in \mathcal{M}_{src} as π_{src}^* , and the in-sample optimal policy (Kostrikov et al., 2021) extracted from the source domain dataset as π_{insrc}^* . We define $\epsilon_{\text{src}}^* := |J_{\mathcal{M}_{\text{src}}}(\pi_{\text{src}}^*) - J_{\mathcal{M}_{\text{src}}}(\pi_{\text{insrc}}^*)|$ to be the statistical error of the inherent performance difference between π_{src}^* and π_{insrc}^* on the source domain, which is constant given a source domain dataset. We aim to minimize the sub-optimality gap of π in the target domain: $\text{SubOpt}(\pi) := |J_{\mathcal{M}_{\text{tar}}}(\pi) - J_{\mathcal{M}_{\text{tar}}}(\pi_{\text{tar}}^*)|$, where π_{tar}^* is the optimal policy in the target domain. We derive the upper bound of this sub-optimality gap in Proposition 4.2.

Proposition 4.2 (Sub-optimality gap on target domain). *Denote the MDP of the source domain and target domain as \mathcal{M}_{src} and \mathcal{M}_{tar} . For a policy $\hat{\pi}$ trained on \mathcal{M}_{src} , the*

sub-optimality gap of $\hat{\pi}$ on \mathcal{M}_{tar} can be bounded as below,

$$\text{SubOpt}(\hat{\pi}) \leq \underbrace{|J_{\mathcal{M}_{\text{src}}}(\hat{\pi}) - J_{\mathcal{M}_{\text{src}}}(\pi_{\text{insrc}}^*)|}_{\text{(a) value misalignment}} + C_2 \cdot \underbrace{\sup_{s,a} [D_{\text{TV}}(P_{\text{src}}(\cdot|s,a), P_{\text{tar}}(\cdot|s,a))] + \epsilon_{\text{src}}^*}_{\text{(b) dynamics misalignment}} \quad (2)$$

where $C_2 = \frac{(2\gamma+2)r_{\text{max}}}{(1-\gamma)^2}$ is a positive constant.

According to Proposition 4.2, the sub-optimality gap in the target domain can be controlled by three terms: (a) *value misalignment*, representing the sub-optimality on the source domain; (b) *dynamics misalignment* as considered in previous works; (c) a constant statistical error ϵ_{src}^* . To tighten such a sub-optimality gap, both dynamics and value misalignment need to be minimized. Hence, we can answer the previous question: *both dynamics and value alignment are essential for efficient cross-domain offline RL.*

5. Dynamics- and Value-Aligned Data Filtering

Proposition 4.2 conveys a promising way to learn a well-performing policy in the target domain: **(1)** minimize the dynamics misalignment between the source domain and target domain; **(2)** minimize the value misalignment between the learned policy and the in-sample optimal policy in the source domain. Neglecting either factor would compromise policy performance. To address this, we adopt a data filtering paradigm inspired by prior works (Xu et al., 2024; Wen et al., 2024; Lyu et al., 2025), which retains source domain data that exhibits aligned dynamics with the target domain, and on which the learned policy can be close to the in-sample optimal policy in the source domain.

5.1. Advantage-Aware Value Alignment

Given that several existing methods can be applied for measuring dynamics misalignment, such as contrastive learning (Wen et al., 2024) and optimal transport (Lyu et al., 2025), the crucial part remains how to capture value misalignment. To tackle this problem, we derive an upper bound of the value misalignment term, which gives us insight for the practical solution.

Proposition 5.1 (Value Misalignment). *Denote the MDP of the source domain and target domain as \mathcal{M}_{src} and \mathcal{M}_{tar} , and the behavior policy of the \mathcal{D}_{src} as μ . For policy $\hat{\pi}$ trained on \mathcal{D}_{src} using an in-sample offline RL algorithm (e.g., IQL), we assume that $(\hat{\pi}(a|s) - \mu(a|s)) A_{\mu}(s, a) \geq 0$. Then the value misalignment in Proposition 4.2 can be upper bounded as follows:*

$$|J_{\mathcal{M}_{\text{src}}}(\hat{\pi}) - J_{\mathcal{M}_{\text{src}}}(\pi_{\text{insrc}}^*)| \leq -\mathbb{E}_{s \sim \rho_{\mu}(\cdot), a \sim \mu(\cdot|s)} [A_{\pi_{\text{insrc}}^*}(s, a)] + \mathcal{O}\left(\frac{1}{(1-\gamma)^2}\right), \quad (3)$$

where $A(s, a)$ is the advantage function, and $\rho_{\mu}(\cdot)$ is the state visiting distribution under μ .

Remark. The assumption $(\hat{\pi}(a|s) - \mu(a|s)) A_{\mu}(s, a) \geq 0$ indicates that, for any state-action pair (s, a) , if $A_{\mu}(s, a) \geq 0$, i.e., the action a shows superiority over average, the policy $\hat{\pi}$ has a higher probability than μ to choose action a , and vice versa. Theoretically, this assumption guarantees that the learned policy $\hat{\pi}$ enjoys a better performance than the behavior policy μ on the source domain (Proposition 4.1 in Liu et al. (2024b)). This is reasonable since the goal of offline RL is to outperform the behavior policy. Furthermore, this assumption can be easily met. If we use IQL (Kostrikov et al., 2021) to optimize the policy $\hat{\pi}$, since IQL utilizes exponential advantage weighted imitation learning, it explicitly updates the policy to favor actions with higher advantage values:

$$\pi_{k+1} = \arg \max_{\pi \in \Pi} \mathbb{E}_{(s,a) \in \mathcal{D}} [\exp(\alpha \cdot A_{\pi_k}(s, a)) \log \pi(a|s)],$$

then if the learned policy π is initialized as μ , after one step of policy update, any (s, a) with $A_{\mu}(s, a) > 0$ will be given more weight for imitation, and vice versa. This naturally satisfies our assumption. Therefore, our assumption is reasonable and easy to meet.

The right-hand side in Equation 3 consists of **(1)** the negative in-sample optimal advantage value on the source domain under the behavior policy’s state-action distribution, and **(2)** a bounded term. Proposition 5.1 gives an important insight that the value misalignment can be upper bounded by the negative advantage value under source domain offline data, estimated by the in-sample optimal advantage function on the source domain. Given that $J_{\mathcal{M}_{\text{src}}}(\hat{\pi}) - J_{\mathcal{M}_{\text{src}}}(\pi_{\text{insrc}}^*) \leq 0$ holds since $\hat{\pi}$ is trained on \mathcal{D}_{src} using an in-sample offline RL algorithm, if we want to minimize the value misalignment, we need to maximize $\mathbb{E}_{s \sim \rho_{\mu}(\cdot), a \sim \mu(\cdot|s)} [A_{\pi_{\text{insrc}}^*}(s, a)]$. This motivates our use of the in-sample optimal advantage function as a quantitative measure for value misalignment, where higher advantage values correspond to lower degrees of value misalignment.

Remark. It is worth noting that VGDF (Xu et al., 2024) also emphasizes the importance of value alignment for cross-domain RL and leverages the value function to guide data filtering. However, DVDF fundamentally differs from VGDF in how it interprets value alignment. VGDF defines value alignment as minimizing $|V(s'_{\text{src}}) - V(s'_{\text{tar}})|$, which quantifies dynamics discrepancy from a value difference perspective. That is, **VGDF still only addresses dynamics mismatch**. In contrast, DVDF minimizes $|J_{\mathcal{M}_{\text{src}}}(\pi) - J_{\mathcal{M}_{\text{src}}}(\pi_{\text{insrc}}^*)|$ for value alignment, which explicitly measures policy optimality in the source domain, orthogonal to the dynamics mismatch. Thus, DVDF comprehensively considers both value and dynamics alignment, thereby distinguishing it from VGDF.

5.2. Practical Implementation

In Section 5.1, we have demonstrated that an in-sample optimal advantage function could be leveraged for capturing value misalignment. The next question is how to obtain such an advantage function. Since we cannot directly acquire the in-sample optimal advantage function, we propose leveraging a pre-trained offline policy trained on the source domain dataset to approximate the in-sample optimal policy, and using its corresponding advantage function to approximate the in-sample optimal advantage function. However, the advantage approximation error is non-negligible and must be minimized. This raises the question of how to perform offline pre-training effectively. We denote the pre-trained policy as π_{pre} , and its advantage function as A_{pre} . We also obtain an advantage function during pre-training, which we denote by \hat{A}_{pre} . Note that A_{pre} and \hat{A}_{pre} are typically different due to the additional conservatism introduced in offline RL. We analyze the advantage approximation error in Proposition 5.2, which provides guidance on how to properly conduct offline pre-training.

Proposition 5.2 (Advantage Approximation Error). *Given a pre-trained policy π_{pre} and advantage function $\hat{A}_{\text{pre}}(\cdot)$ to approximate the in-sample optimal policy π_{insrc}^* and in-sample optimal advantage function $A_{\pi_{\text{insrc}}^*}(\cdot)$, then the advantage approximation error on offline samples generated by the behavior policy μ is*

$$\mathbb{E}_{s \sim \rho_{\mu}(\cdot), a \sim \mu(\cdot|s)} \left[\hat{A}_{\text{pre}}(s, a) - A_{\pi_{\text{insrc}}^*}(s, a) \right] = \Delta J_{\mathcal{M}_{\text{src}}}(\pi_{\text{insrc}}^*, \pi_{\text{pre}}) + \mathbb{E}_{s \sim \rho_{\mu}(\cdot), a \sim \mu(\cdot|s)} [\Delta(s, a)], \quad (4)$$

with $\Delta J_{\mathcal{M}_{\text{src}}}(\pi_{\text{insrc}}^*, \pi_{\text{pre}}) = J_{\mathcal{M}_{\text{src}}}(\pi_{\text{insrc}}^*) - J_{\mathcal{M}_{\text{src}}}(\pi_{\text{pre}})$, and $\Delta(s, a) = \hat{A}_{\text{pre}}(s, a) - A_{\text{pre}}(s, a)$.

Proposition 5.2 suggests that minimizing the advantage approximation error requires selecting an offline RL algorithm with two properties: (1) strong empirical performance (to minimize $\Delta J_{\mathcal{M}_{\text{src}}}(\pi_{\text{insrc}}^*, \pi_{\text{pre}})$), and (2) accurate advantage estimation (such that $\Delta(s, a)$ is minimized). Although IQL is a natural candidate due to its ability to achieve near in-sample optimal performance across diverse benchmarks and its straightforward advantage estimation, its known tendency for V -function underestimation (caused by suboptimal actions) (Xu et al., 2023; Chen et al., 2025) may compromise advantage accuracy and consequently mislead data filtering. To address this limitation while maintaining high performance, we instead adopt another offline RL algorithm, Sparse Q-Learning (SQL) (Xu et al., 2023), for pre-training. As an in-sample learning algorithm that explicitly enforces policy sparsity, SQL achieves both near in-sample optimal performance and more reliable advantage estimates, thereby better satisfying our dual requirements of algorithmic performance and advantage accuracy.

After pre-training, we obtain a Q -function $\hat{Q}_{\text{pre}}(s, a)$ and a

V -function $\hat{V}_{\text{pre}}(s)$, we directly derive the advantage function as $\hat{A}_{\text{pre}}(s, a) = \hat{Q}_{\text{pre}}(s, a) - \hat{V}_{\text{pre}}(s)$. Then, we can leverage the pre-trained advantage function as an indicator of value misalignment. The next step is to choose the indicator of the dynamics misalignment. We can just follow previous studies, and apply methods such as contrastive learning (Wen et al., 2024) and optimal transport (Lyu et al., 2025). Here, we follow IGDF (Wen et al., 2024) and measure dynamics misalignment via contrastive learning. Specifically, we train a score function $h(s, a, s')$ via the NCE loss:

$$\mathcal{L}_{\text{NCE}} = -\mathbb{E}_{(s, a, s'_{\text{tar}})} \mathbb{E}_{S'_{\text{src}}} \left[\log \frac{h(s, a, s'_{\text{tar}})}{\sum_{s' \in \{s'_{\text{tar}}\} \cup S'_{\text{src}}} h(s, a, s')} \right],$$

where S'_{src} represents the next states from the source dataset. Intuitively, $h(s, a, s')$ assigns high scores when $s' \sim P_{\mathcal{M}_{\text{tar}}}(\cdot|s, a)$, and assigns low scores when $(s, a) \in \mathcal{D}_{\text{tar}}$ and $s' \in \mathcal{D}_{\text{src}}$. Hence, $h(s, a, s')$ can reflect whether the dynamics of the transition (s, a, s') aligns with the target domain dynamics.

Based on the pre-trained advantage function $\hat{A}_{\text{pre}}(\cdot)$ and score function $h(\cdot)$, we propose a practical algorithm, termed DVDF (**D**ynamics- and **V**alue-aligned **D**ata **F**iltering), which selectively shares source domain data with smaller dynamics and value misalignment to train a target policy. Specifically, we define a new score function $g(s, a, s')$ as follows:

$$g(s, a, s') = \lambda \cdot h(s, a, s') + (1 - \lambda) \cdot \text{Norm}(\hat{A}_{\text{pre}}(s, a)), \quad (5)$$

where λ is a tunable hyperparameter, and $\text{Norm}(\cdot)$ is the min-max normalization operator. $g(\cdot)$ balances value and dynamics misalignment through a simple weighted summation strategy. **This design directly aligns with our theoretical results in Proposition 4.2**, which also combines the two terms via a weighted summation. Then, we extract the top ξ -quantile of batch source samples for training, and weigh the Temporal-Difference (TD)-error of selected source data using the score function as in (Wen et al., 2024):

$$\mathcal{L}_Q(\theta) = \frac{1}{2} \mathbb{E}_{(s, a, s') \sim \mathcal{D}_{\text{tar}}} [(Q_{\theta} - \mathcal{T}Q_{\theta})^2] + \frac{1}{2} \mathbb{E}_{(s, a, s') \sim \mathcal{D}_{\text{src}}} [w(s, a, s') g(s, a, s') (Q_{\theta} - \mathcal{T}Q_{\theta})^2], \quad (6)$$

where $w(s, a, s') = \mathbb{I}(g(s, a, s') > g_{\xi\%})$ is an indicator function, and $g_{\xi\%}$ means the ξ -th quantile of the g -values among source domain samples in a batch. The last step is to update the policy via offline RL algorithms such as IQL. Note that DVDF can serve as a plug-in module and can be combined with different cross-domain offline RL algorithms such as IGDF and OTDF (Lyu et al., 2025), yielding DVDF-IGDF and DVDF-OTDF. We present the detailed algorithm procedure of DVDF-IGDF and DVDF-OTDF in Appendix D.3.

Table 1. Performance comparison under kinematic shifts. half=halfcheetah, hopp=hopper, walk=walker2d, r=random, m=medium, me=medium-expert, mr=medium-replay, e=expert. We report the normalized score evaluated in the target domain after 1M steps of training, and \pm captures the standard deviation across 5 seeds. We **bold** the highest scores for each task.

Dataset	IQL	BOSA	DARA	IGDF	DVDF-IGDF	OTDF	DVDF-OTDF
half-r	4.9	2.2	4.7	5.4±0.4	4.6±0.1	2.2±0.2	1.7±0.1
half-m	45.2	39.6	44.1	45.2±0.1	45.1±0.2	42.2±0.1	45.4±0.6
half-mr	22.1	26.3	21.6	22.9±1.4	26.6±2.3	15.6±3.1	26.8±4.4
half-me	43.7	42.2	52.7	57.1±8.9	66.7±6.3	46.7±4.4	45.9±3.0
half-e	49.7	84.3	47.4	47.6±2.1	58.8±4.7	79.6±3.0	88.9±5.6
hopp-r	4.5	40.7	3.8	13.0±1.9	3.3±0.1	2.9±0.4	12.6±0.1
hopp-m	48.8	71.4	48.8	54.3±6.6	59.1±3.4	46.3±3.7	67.8±4.1
hopp-mr	40.2	29.5	41.6	30.0±5.2	32.1±0.8	26.2±4.4	44.7±2.2
hopp-me	12.5	49.6	17.0	11.6±0.6	60.2±5.9	58.1±4.9	70.2±7.7
hopp-e	62.6	94.8	59.1	70.1±3.2	83.9±5.0	97.0±3.3	111.8±4.5
walk-r	4.0	2.2	5.1	5.2±0.3	9.8±1.7	0.0±0.0	0.0±0.0
walk-m	48.7	44.5	43.4	51.8±2.4	69.7±4.4	43.0±2.1	71.6±5.9
walk-mr	12.6	4.8	15.6	11.2±1.1	22.6±1.8	10.7±1.9	25.6±2.4
walk-me	95.4	35.1	85.3	90.6±3.4	104.6±5.1	63.1±6.6	91.6±8.2
walk-e	90.1	41.9	85.5	93.7±5.8	108.0±4.3	98.9±2.1	106.0±1.2
ant-r	11.5	31.5	10.9	13.7±1.9	15.6±2.2	11.6±1.0	25.7±3.4
ant-m	89.9	28.4	98.9	88.0±4.6	98.1±5.0	86.1±3.7	97.1±5.0
ant-mr	46.8	22.0	42.1	58.2±9.7	44.1±7.6	39.6±8.1	36.8±3.9
ant-me	106.1	102.5	104.8	112.8±4.0	126.6±7.4	105.1±3.9	117.2±6.1
ant-e	111.0	57.6	115.1	119.2±5.6	125.2±3.9	111.6±2.9	107.9±4.0
Total	950.3	851.1	947.5	1001.6	1164.7	986.5	1172.3

6. Experiments

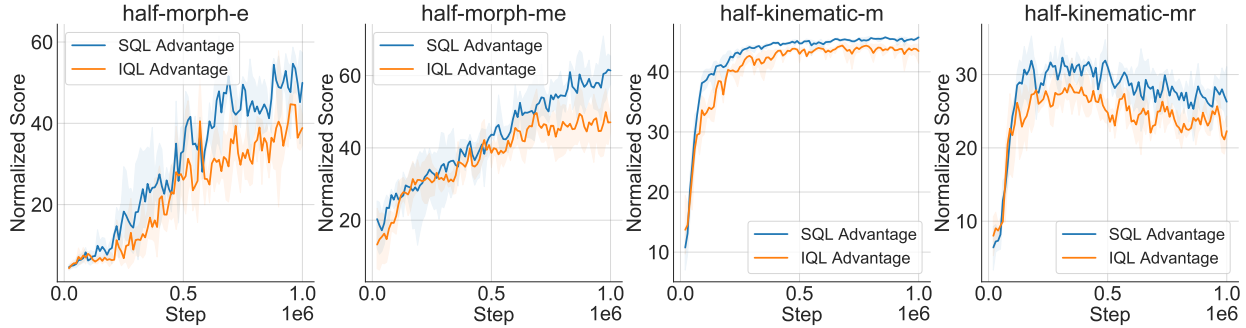
In this section, we examine the effectiveness of our proposed method by conducting extensive experiments on environments with various challenging dynamics shifts. We compare the performance of DVDF and other baselines in Section 6.1, and empirically show that DVDF achieves effective offline policy adaptation and consistently outperforms prior strong baselines across varied dynamics shifts and dataset qualities. In Section 6.2 and Section 6.3, we conduct a detailed ablation study and parameter study for a better understanding of DVDF.

6.1. Main Results under Various Dynamics Shifts

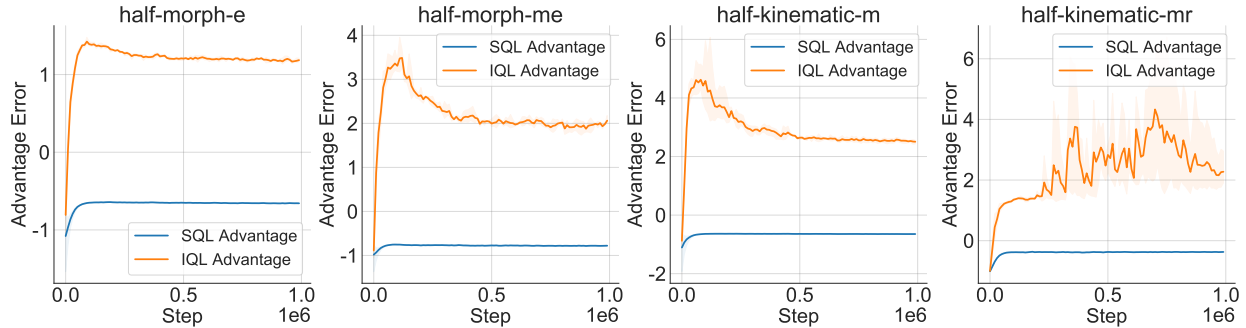
Tasks and Datasets. For the types of dynamics shifts, we consider kinematic shifts and morphology shifts in this paper, and the dynamics shifts are applied to four tasks (halfcheetah, hopper, walker2d, ant) from OpenAI Gym (Brockman et al., 2016). The kinematic shifts are realized by reducing the rotation range of some joints, and the morphology shifts are simulated by modifying the size of some limbs. We defer more details for the realization of dynamics shifts to Appendix C.2 and C.3. Since only a limited amount of target data is accessible, we can sample a percentage of data from offline datasets from D4RL (Fu et al.,

2020) as the target domain datasets. We set the percentage to 10% in our experiments. For source domain datasets, we collect data in the modified environments, following a similar data collection process as D4RL. Specifically, we collect datasets of five data qualities (random, medium, medium-replay, medium-expert, expert) with an SAC (Haarnoja et al., 2018) agent trained to different levels of performance in the respective environments, and each source domain dataset contains around 1M samples, much more than the target domain datasets. This amounts to a total of **40** source domain datasets and **20** target domain datasets. Note that for each pair of source and target domain datasets, the type of tasks and dataset quality remain the same, and the difference lies in the transition dynamics and the dataset size. We also examine DVDF in extremely low-data settings (Lyu et al., 2025) where the target dataset contains only 5,000 transitions. We defer the results in Appendix E.2.

Baselines. We choose the following baselines for comparison: **IQL** (Kostrikov et al., 2021) (which we train directly on the mixture of source domain data and target domain data), **BOSA** (Liu et al., 2024a), **DARA** (Liu et al., 2022), **IGDF** (Wen et al., 2024) and **OTDF** (Lyu et al., 2025). The backbone of IGDF and OTDF is IQL. We exclude VGDF (Xu et al., 2024) as our baseline since it requires an



(a) Performance comparison with SQL and IQL pre-trained advantage function.



(b) Advantage estimation error comparison with SQL and IQL pre-trained advantage function.

Figure 2. Ablation study on SQL pre-trained advantage function.

online target environment. More details about these baselines are presented in Appendix D.1. For our method, we implement DVDF-IGDF and DVDF-OTDF for comparison.

Experimental Results. We present the comparison results for each method under kinematic shifts in Table 1. Due to space limit, the results under morphology shifts are deferred to Appendix E.1. We report the normalized score in the target domain. Empirical results demonstrate that DVDF consistently enhances the performance of base algorithms (IGDF and OTDF) while outperforming more baselines (IQL, BOSA, and DARA) across diverse tasks and dataset qualities under kinematic shifts. Notably, DVDF-IGDF surpasses IGDF on **16** out of 20 tasks under kinematic shifts, and DVDF-OTDF achieves a higher score than OTDF on **15** out of 20 tasks under kinematic shifts. Adopting DVDF incurs an increase of **16.3%** (from 1001.6 to 1164.7) and **18.8%** (from 986.5 to 1172.3) to IGDF and OTDF respectively, in terms of the total normalized score under kinematic shifts. Moreover, DVDF shows superiority especially on datasets containing high-quality samples (medium-expert and expert), outperforming IGDF on **8** out of 8 tasks and OTDF on **6** out of 8 tasks. We attribute this to DVDF’s ability to select dynamics- and value-aligned source domain data, whereas IGDF and OTDF may discard substantial value-aligned data, which inevitably limits their potential for effective policy transfer.

6.2. Ablation Study

In this section, we examine the necessity of SQL pre-training for obtaining the advantage function. We pre-train both SQL and IQL, and apply the resulting advantage functions for data filtering. Experiments are conducted on four datasets using DVDF-IGDF as the base algorithm, with other settings consistent with Section 6.1. We compare the two pre-training methods in terms of algorithm performance and advantage estimation error.

Performance Comparison. Figure 2 (a) shows the learning curves and performance comparison on four datasets using SQL and IQL pre-trained advantage functions. Clearly, employing the SQL pre-trained advantage function for data filtering yields better performance than using IQL. Therefore, we use the advantage function obtained by SQL pre-training for data filtering in our experiments.

Advantage Estimation Error Comparison. We next examine whether the performance improvement from SQL pre-training stems from a more accurate advantage function. We define the advantage estimation error as $\mathcal{E} = \mathbb{E}_{(s,a) \in \mathcal{D}_{\text{src}}} \frac{\hat{A}(s,a) - A(s,a)}{A(s,a)}$, where $\hat{A}(\cdot)$ is the estimated advantage function by either SQL or IQL, and $A(\cdot)$ is the true advantage function obtained by Monte Carlo rollouts. Figure 2 (b) shows the advantage estimation error com-

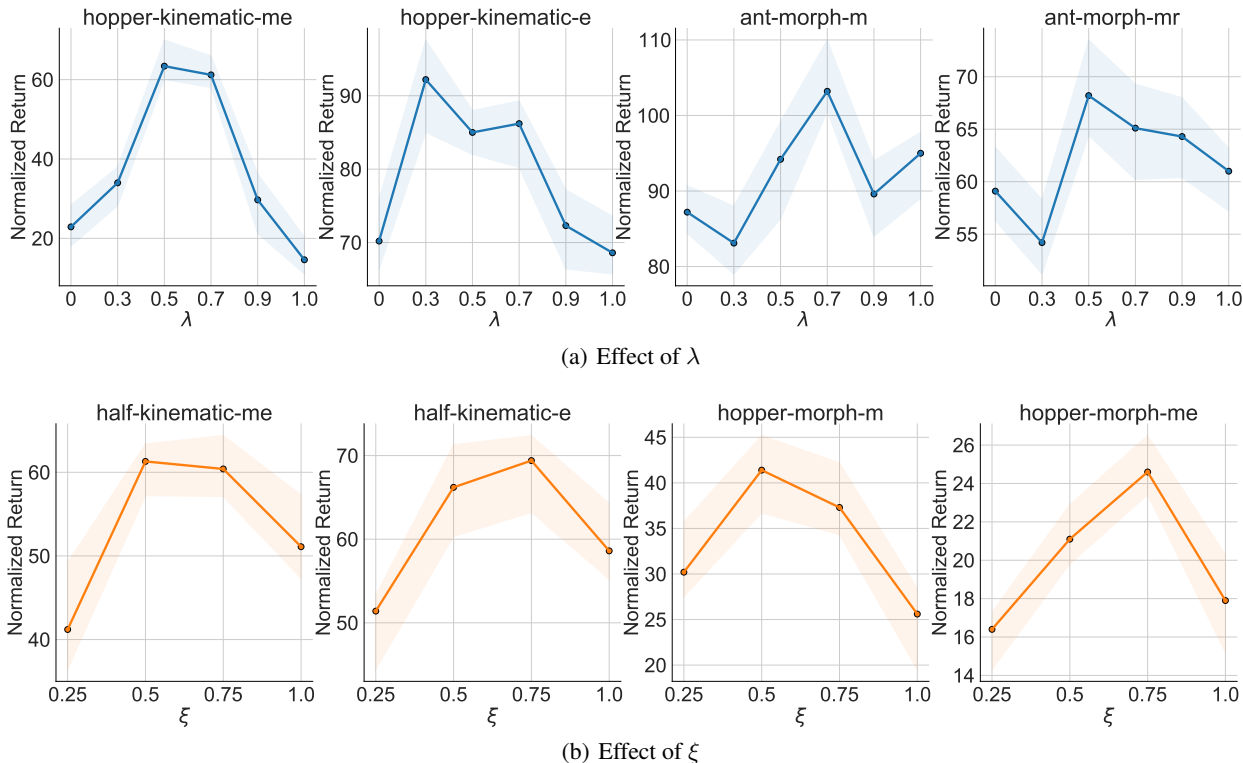


Figure 3. Parameter sensitivity experiments on λ and ξ .

parison during pre-training. We observe that IQL quickly overestimates the advantage value, consistent with (Xu et al., 2023), noting that IQL tends to underestimate the V -function, thereby inflating the estimated advantage. In contrast, SQL typically underestimates the advantage due to the sparsity induced in V -function learning. Nevertheless, SQL maintains a smaller estimation error than IQL throughout pre-training, indicating that SQL provides more accurate advantage estimation.

6.3. Parameter Sensitivity

In this section, we investigate the sensitivity of DVDF to the hyperparameters. There are two main hyperparameters in DVDF: the data selection ratio ξ and the alignment tradeoff coefficient λ . We choose DVDF-IGDF as our base algorithm, running for 1M steps with 10 random seeds. The dataset setting follows Section 6.1.

Alignment tradeoff coefficient λ . The parameter λ balances the weight of dynamics alignment and value alignment during data filtering. A larger λ emphasizes more on dynamics alignment, and vice versa. We vary λ across $\{0.0, 0.3, 0.5, 0.7, 0.9, 1.0\}$ and conduct experiments on four different tasks. Figure 3 (a) shows the impact of different values of λ on the final performance, which indicates that neither excessive emphasis on dynamics alignment nor value alignment represents the best choice, and $\lambda = 0.7$

could achieve an effective trade-off between dynamics and value alignment. Therefore, we fix $\lambda = 0.7$ across all datasets in our experiments without further tuning.

Data selection ratio ξ . The parameter ξ decides how many source domain samples can be shared. A larger ξ implies more source domain samples are accepted. To examine its influence, we conduct experiments on four tasks. We sweep ξ across $\{0.25, 0.5, 0.75, 1.0\}$ and present the final performance comparison in Figure 3 (b). We observe an inferior performance when $\xi = 0.25$ or $\xi = 1.0$, and setting $\xi = 0.5$ could achieve a favorable result on most tasks. Therefore, we set $\xi = 0.5$ uniformly for DVDF in all the experiments, instead of performing task-specific tuning.

7. Conclusion

In this paper, through empirical and theoretical analyses, we demonstrate that both dynamics alignment and value alignment are critical for efficient cross-domain offline RL. Building upon this insight, we propose a novel method, DVDF, which leverages a pretrained advantage function to quantify value misalignment and performs data filtering by jointly considering dynamics and value misalignment, filling a gap in prior research. Extensive experiments across various dynamics shift scenarios and tasks demonstrate that DVDF outperforms prior strong baselines and brings significant performance improvement to base algorithms.

Impact Statement

This paper presents work whose goal is to advance the field of Machine Learning. There are many potential societal consequences of our work, none of which we feel must be specifically highlighted here.

References

- Achiam, J., Held, D., Tamar, A., and Abbeel, P. Constrained policy optimization. In *International conference on machine learning*, pp. 22–31. PMLR, 2017.
- Brockman, G., Cheung, V., Pettersson, L., Schneider, J., Schulman, J., Tang, J., and Zaremba, W. Openai gym. *arXiv preprint arXiv:1606.01540*, 2016.
- Chae, J., Han, S., Jung, W., Cho, M., Choi, S., and Sung, Y. Robust imitation learning against variations in environment dynamics. In *International Conference on Machine Learning*, pp. 2828–2852. PMLR, 2022.
- Chen, T., Cai, R., Wu, F., and Zhang, X. Active: Offline reinforcement learning via adaptive imitation and in-sample v -ensemble. In *The Thirteenth International Conference on Learning Representations*, 2025.
- Cheng, C.-A., Xie, T., Jiang, N., and Agarwal, A. Adversarially trained actor critic for offline reinforcement learning. In *International Conference on Machine Learning*, pp. 3852–3878. PMLR, 2022.
- Clavera, I., Nagabandi, A., Fearing, R. S., Abbeel, P., Levine, S., and Finn, C. Learning to adapt: Meta-learning for model-based control. *arXiv preprint arXiv:1803.11347*, 3:3, 2018.
- Csiszár, I. and Körner, J. *Information theory: coding theorems for discrete memoryless systems*. Cambridge University Press, 2011.
- Cuturi, M., Meng-Papaxanthos, L., Tian, Y., Bunne, C., Davis, G., and Teboul, O. Optimal transport tools (ott): A jax toolbox for all things wasserstein. *arXiv preprint arXiv:2201.12324*, 2022.
- Du, Y., Watkins, O., Darrell, T., Abbeel, P., and Pathak, D. Auto-tuned sim-to-real transfer. In *2021 IEEE International Conference on Robotics and Automation (ICRA)*, pp. 1290–1296. IEEE, 2021.
- Eysenbach, B., Asawa, S., Chaudhari, S., Levine, S., and Salakhutdinov, R. Off-dynamics reinforcement learning: Training for transfer with domain classifiers. *arXiv preprint arXiv:2006.13916*, 2020.
- Finn, C., Abbeel, P., and Levine, S. Model-agnostic meta-learning for fast adaptation of deep networks. In *International conference on machine learning*, pp. 1126–1135. PMLR, 2017.
- Fu, J., Kumar, A., Nachum, O., Tucker, G., and Levine, S. D4rl: Datasets for deep data-driven reinforcement learning. *arXiv preprint arXiv:2004.07219*, 2020.
- Fujimoto, S. and Gu, S. S. A minimalist approach to offline reinforcement learning. *Advances in neural information processing systems*, 34:20132–20145, 2021.
- Fujimoto, S., Meger, D., and Precup, D. Off-policy deep reinforcement learning without exploration. In *International conference on machine learning*, pp. 2052–2062. PMLR, 2019.
- Guo, Y., Wang, Y., Shi, Y., Xu, P., and Liu, A. Off-dynamics reinforcement learning via domain adaptation and reward augmented imitation. *Advances in Neural Information Processing Systems*, 37:136326–136360, 2024.
- Guo, Y., Yang, Y., Xu, P., and Liu, A. Mobody: Model based off-dynamics offline reinforcement learning. *arXiv preprint arXiv:2506.08460*, 2025.
- Haarnoja, T., Zhou, A., Abbeel, P., and Levine, S. Soft actor-critic: Off-policy maximum entropy deep reinforcement learning with a stochastic actor. In *International conference on machine learning*, pp. 1861–1870. Pmlr, 2018.
- Ji, T., Luo, Y., Sun, F., Jing, M., He, F., and Huang, W. When to update your model: Constrained model-based reinforcement learning. *Advances in neural information processing systems*, 35:23150–23163, 2022.
- Jin, Y., Yang, Z., and Wang, Z. Is pessimism provably efficient for offline rl? In *Proceedings of the 38th International Conference on Machine Learning*, pp. 5084–5096, 2021.
- Kakade, S. and Langford, J. Approximately optimal approximate reinforcement learning. In *Proceedings of the Nineteenth International Conference on Machine Learning*, pp. 267–274, 2002.
- Kidambi, R., Rajeswaran, A., Netrapalli, P., and Joachims, T. Morel: Model-based offline reinforcement learning. *Advances in neural information processing systems*, 33: 21810–21823, 2020.
- Kim, K., Gu, Y., Song, J., Zhao, S., and Ermon, S. Domain adaptive imitation learning. In *International Conference on Machine Learning*, pp. 5286–5295. PMLR, 2020.
- Kingma, D. P. Adam: A method for stochastic optimization. *arXiv preprint arXiv:1412.6980*, 2014.

- Kingma, D. P., Welling, M., et al. Auto-encoding variational bayes, 2013.
- Kober, J., Bagnell, J. A., and Peters, J. Reinforcement learning in robotics: A survey. *The International Journal of Robotics Research*, 32(11):1238–1274, 2013.
- Kormushev, P., Calinon, S., and Caldwell, D. G. Reinforcement learning in robotics: Applications and real-world challenges. *Robotics*, 2(3):122–148, 2013.
- Kostrikov, I., Nair, A., and Levine, S. Offline reinforcement learning with implicit q-learning. *arXiv preprint arXiv:2110.06169*, 2021.
- Kumar, A., Fu, J., Soh, M., Tucker, G., and Levine, S. Stabilizing off-policy q-learning via bootstrapping error reduction. *Advances in neural information processing systems*, 32, 2019.
- Kumar, A., Zhou, A., Tucker, G., and Levine, S. Conservative q-learning for offline reinforcement learning. *Advances in neural information processing systems*, 33: 1179–1191, 2020.
- Langley, P. Crafting papers on machine learning. In Langley, P. (ed.), *Proceedings of the 17th International Conference on Machine Learning (ICML 2000)*, pp. 1207–1216, Stanford, CA, 2000. Morgan Kaufmann.
- Le Pham Van, L., Nguyen, M. H., Kieu, D., Le, H., Gupta, S., et al. Dmc: Nearest neighbor guidance diffusion model for offline cross-domain reinforcement learning. In *ECAI 2025*, pp. 2331–2338. IOS Press, 2025.
- Levine, S., Kumar, A., Tucker, G., and Fu, J. Offline reinforcement learning: Tutorial, review, and perspectives on open problems. *arXiv preprint arXiv:2005.01643*, 2020.
- Liu, J., Zhang, H., and Wang, D. Dara: Dynamics-aware reward augmentation in offline reinforcement learning. *arXiv preprint arXiv:2203.06662*, 2022.
- Liu, J., Zhang, Z., Wei, Z., Zhuang, Z., Kang, Y., Gai, S., and Wang, D. Beyond ood state actions: Supported cross-domain offline reinforcement learning. In *Proceedings of the AAAI Conference on Artificial Intelligence*, volume 38, pp. 13945–13953, 2024a.
- Liu, T., Li, Y., Lan, Y., Gao, H., Pan, W., and Xu, X. Adaptive advantage-guided policy regularization for offline reinforcement learning. In *International Conference on Machine Learning*, pp. 31406–31424. PMLR, 2024b.
- Liu, T., Li, J., Zheng, Y., Niu, H., Lan, Y., Xu, X., and Zhan, X. Skill expansion and composition in parameter space. In *The Thirteenth International Conference on Learning Representations*, 2025.
- Lyu, J., Ma, X., Li, X., and Lu, Z. Mildly conservative q-learning for offline reinforcement learning. *Advances in Neural Information Processing Systems*, 35:1711–1724, 2022.
- Lyu, J., Bai, C., Yang, J., Lu, Z., and Li, X. Cross-domain policy adaptation by capturing representation mismatch. *arXiv preprint arXiv:2405.15369*, 2024a.
- Lyu, J., Xu, K., Xu, J., Yan, M., Yang, J., Zhang, Z., Bai, C., Lu, Z., and Li, X. Odrl: A benchmark for off-dynamics reinforcement learning. In *The Thirty-eight Conference on Neural Information Processing Systems Datasets and Benchmarks Track*, 2024b. URL <https://openreview.net/forum?id=ap4x1kArGy>.
- Lyu, J., Yan, M., Qiao, Z., Liu, R., Ma, X., Ye, D., Yang, J.-W., Lu, Z., and Li, X. Cross-domain offline policy adaptation with optimal transport and dataset constraint. In *The Thirteenth International Conference on Learning Representations*, 2025.
- Mehta, B., Diaz, M., Golemo, F., Pal, C. J., and Paull, L. Active domain randomization. In *Conference on Robot Learning*, pp. 1162–1176. PMLR, 2020.
- Mnih, V., Kavukcuoglu, K., Silver, D., Graves, A., Antonoglou, I., Wierstra, D., and Riedmiller, M. Playing atari with deep reinforcement learning. *arXiv preprint arXiv:1312.5602*, 2013.
- Nagabandi, A., Clavera, I., Liu, S., Fearing, R. S., Abbeel, P., Levine, S., and Finn, C. Learning to adapt in dynamic, real-world environments through meta-reinforcement learning. *arXiv preprint arXiv:1803.11347*, 2018.
- Nikulin, A., Kurenkov, V., Tarasov, D., and Kolesnikov, S. Anti-exploration by random network distillation. In *International Conference on Machine Learning*, pp. 26228–26244. PMLR, 2023.
- Niu, H., Qiu, Y., Li, M., Zhou, G., Hu, J., Zhan, X., et al. When to trust your simulator: Dynamics-aware hybrid offline-and-online reinforcement learning. *Advances in Neural Information Processing Systems*, 35: 36599–36612, 2022.
- Niu, H., Ji, T., Liu, B., Zhao, H., Zhu, X., Zheng, J., Huang, P., Zhou, G., Hu, J., and Zhan, X. H2o+: an improved framework for hybrid offline-and-online rl with dynamics gaps. *arXiv preprint arXiv:2309.12716*, 2023.
- Pan, K.-C., Chen, M., Liu, X., and Hsieh, P.-C. Survive on planet pandora: Robust cross-domain rl under distinct state-action representations. In *ICML 2024 Workshop: Aligning Reinforcement Learning Experimentalists and Theorists*.

- Peyré, G., Cuturi, M., et al. Computational optimal transport: With applications to data science. *Foundations and Trends® in Machine Learning*, 11(5-6):355–607, 2019.
- Prudencio, R. F., Maximo, M. R., and Colombini, E. L. A survey on offline reinforcement learning: Taxonomy, review, and open problems. *IEEE Transactions on Neural Networks and Learning Systems*, 35(8):10237–10257, 2023.
- Puterman, M. L. Markov decision processes. *Handbooks in operations research and management science*, 2:331–434, 1990.
- Qiao, Z., Lyu, J., Jiao, K., Liu, Q., and Li, X. Sumo: Search-based uncertainty estimation for model-based offline reinforcement learning. In *Proceedings of the AAAI Conference on Artificial Intelligence*, volume 39, pp. 20033–20041, 2025.
- Qiao, Z., Lyu, J., Lyu, B., Shu, Y., Gao, S., and Qiu, S. Model-based offline rl via robust value-aware model learning with implicitly differentiable adaptive weighting. In *The Fourteenth International Conference on Learning Representations*, 2026a.
- Qiao, Z., Yang, R., Lyu, J., Li, X., Dai, Z., Yang, Z., Gao, S., and Qiu, S. Dual-robust cross-domain offline reinforcement learning against dynamics shifts. In *The Fourteenth International Conference on Learning Representations*, 2026b.
- Rashidinejad, P., Zhu, B., Ma, C., Jiao, J., and Russell, S. Bridging offline reinforcement learning and imitation learning: A tale of pessimism. *IEEE Transactions on Information Theory*, 68(12):8156–8196, 2022.
- Slaoui, R. B., Clements, W. R., Foerster, J. N., and Toth, S. Robust domain randomization for reinforcement learning. 2019.
- Sutton, R. S. and Barto, A. G. Reinforcement learning: An introduction. *Robotica*, 17(2):229–235, 1999.
- Todorov, E., Erez, T., and Tassa, Y. Mujoco: A physics engine for model-based control. In *2012 IEEE/RSJ international conference on intelligent robots and systems*, pp. 5026–5033. IEEE, 2012.
- Van der Maaten, L. and Hinton, G. Visualizing data using t-sne. *Journal of machine learning research*, 9(11), 2008.
- Wang, R., Yang, Y., Liu, Z., Zhou, D., and Xu, P. Return augmented decision transformer for off-dynamics reinforcement learning. *arXiv preprint arXiv:2410.23450*, 2024.
- Wen, X., Bai, C., Xu, K., Yu, X., Zhang, Y., Li, X., and Wang, Z. Contrastive representation for data filtering in cross-domain offline reinforcement learning. *arXiv preprint arXiv:2405.06192*, 2024.
- Wu, Y., Zhai, S., Srivastava, N., Susskind, J., Zhang, J., Salakhutdinov, R., and Goh, H. Uncertainty weighted actor-critic for offline reinforcement learning. *arXiv preprint arXiv:2105.08140*, 2021.
- Xu, H., Li, Y., Tian, Y., Darrell, T., and Ma, T. Algorithmic framework for model-based reinforcement learning with theoretical guarantees. *arXiv preprint arXiv:1807.03858*, 2018.
- Xu, H., Jiang, L., Li, J., Yang, Z., Wang, Z., Chan, V. W. K., and Zhan, X. Offline rl with no ood actions: In-sample learning via implicit value regularization. *arXiv preprint arXiv:2303.15810*, 2023.
- Xu, K., Bai, C., Ma, X., Wang, D., Zhao, B., Wang, Z., Li, X., and Li, W. Cross-domain policy adaptation via value-guided data filtering. *Advances in Neural Information Processing Systems*, 36, 2024.
- Xue, Z., Cai, Q., Liu, S., Zheng, D., Jiang, P., Gai, K., and An, B. State regularized policy optimization on data with dynamics shift. *Advances in neural information processing systems*, 36:32926–32937, 2023.
- Yan, M., Lyu, J., Sun, S., Qiao, Z., Yang, J., Lin, Z., Ye, D., and Li, X. Cross-domain offline policy adaptation via selective transition correction. *arXiv preprint arXiv:2602.05776*, 2026.
- Ye, D., Liu, Z., Sun, M., Shi, B., Zhao, P., Wu, H., Yu, H., Yang, S., Wu, X., Guo, Q., et al. Mastering complex control in moba games with deep reinforcement learning. In *Proceedings of the AAAI Conference on Artificial Intelligence*, 2020.
- Yu, T., Thomas, G., Yu, L., Ermon, S., Zou, J. Y., Levine, S., Finn, C., and Ma, T. Mopo: Model-based offline policy optimization. *Advances in Neural Information Processing Systems*, 33:14129–14142, 2020.
- Yu, T., Kumar, A., Rafailov, R., Rajeswaran, A., Levine, S., and Finn, C. Combo: Conservative offline model-based policy optimization. *Advances in neural information processing systems*, 34:28954–28967, 2021.
- Zhang, D., Lyu, B., Qiu, S., mladen kolar, and Zhang, T. Pessimism meets risk: Risk-sensitive offline reinforcement learning. In *Forty-first International Conference on Machine Learning*, 2024.

A. Related Works

Offline RL. Typical offline RL (Levine et al., 2020; Prudencio et al., 2023) assumes only access to a static dataset collected in the target environment. Value overestimation may occur in offline RL due to the OOD action issue (Kumar et al., 2020; Fujimoto et al., 2019; Fujimoto & Gu, 2021). Common solutions for this issue include conservative value estimation (Kumar et al., 2020; Lyu et al., 2022; Nikulin et al., 2023; Cheng et al., 2022; Jin et al., 2021; Zhang et al., 2024; Rashidinejad et al., 2022), adding policy constraints (Kumar et al., 2019; Fujimoto & Gu, 2021; Wu et al., 2021), and augmenting the dataset with dynamics models (Yu et al., 2020; 2021; Kidambi et al., 2020; Qiao et al., 2026a; 2025). Our focus is different from these works since we leverage data from another source domain for policy learning.

Domain Adaptation in RL. In this work, we investigate the cross-domain policy adaptation problem under dynamics shifts (Xu et al., 2024; Lyu et al., 2024a; Xue et al., 2023; Yan et al., 2026; Qiao et al., 2026b), while keeping other MDP components unchanged. Previous studies for this problem include domain randomization (Slaoui et al., 2019; Mehta et al., 2020), system identification (Clavera et al., 2018; Du et al., 2021), imitation learning (Chae et al., 2022; Kim et al., 2020), and meta RL (Finn et al., 2017; Nagabandi et al., 2018). However, these methods require a manipulable simulator or expert trajectories from the target domain. Recent works (Pan et al.; Guo et al., 2024; 2025; Wang et al., 2024; Niu et al., 2022; 2023) dismiss these limitations and study the setting where limited target domain data and sufficient source domain data are available, either online or offline. Instead, we focus on a cross-domain offline RL setting, where both source and target domain data are offline. In this setting, recent studies include reward modification through domain classifier (Liu et al., 2022) or decision transformer (Wang et al., 2024), utilizing supported value optimization (Liu et al., 2024a), leveraging contrastive representation (Wen et al., 2024) or optimal transport (Lyu et al., 2025) for data filtering, and so on. In addition, PSEC (Liu et al., 2025) achieves effective policy adaptation by dynamically composing the parameters of pre-trained source and target domain policies, DmC (Le Pham Van et al., 2025) employs a KNN-based estimator as a measure of dynamics gap, and utilizes the KNN proximity score as a guiding signal for diffusion-based data augmentation. These works have primarily focused on dynamics alignment while neglecting the critical role of value alignment in the source domain. In contrast, DVDF jointly considers dynamics and value alignment, filling this gap in prior research.

B. Proofs of Theoretical Results

In this section, we provide the detailed proofs of the theoretical results in the main text.

B.1. Proof of Lemma 4.1

Proof. The proof starts with

$$\begin{aligned}
 |J_{\mathcal{M}_{\text{tar}}}(\pi) - J_{\mathcal{M}_{\text{src}}}(\pi)| &= \left| \frac{\gamma}{1-\gamma} \mathbb{E}_{s,a \sim \rho_{\mathcal{M}_{\text{tar}}}^{\pi}} [\mathbb{E}_{s' \sim P_{\text{tar}}} [V_{\mathcal{M}_{\text{src}}}^{\pi}(s')] - \mathbb{E}_{s' \sim P_{\text{src}}} [V_{\mathcal{M}_{\text{src}}}^{\pi}(s')]] \right| \\
 &= \left| \frac{\gamma}{1-\gamma} \mathbb{E}_{s,a \sim \rho_{\mathcal{M}_{\text{tar}}}^{\pi}} \left[\int_{s'} (P_{\text{tar}}(s'|s,a) - P_{\text{src}}(s'|s,a)) V_{\mathcal{M}_{\text{src}}}^{\pi}(s') \right] \right| \\
 &\leq \frac{\gamma}{1-\gamma} \mathbb{E}_{s,a \sim \rho_{\mathcal{M}_{\text{tar}}}^{\pi}} \left[\int_{s'} |P_{\text{tar}}(s'|s,a) - P_{\text{src}}(s'|s,a)| V_{\mathcal{M}_{\text{src}}}^{\pi}(s') \right] \\
 &\leq \frac{\gamma \cdot r_{\max}}{(1-\gamma)^2} \mathbb{E}_{s,a \sim \rho_{\mathcal{M}_{\text{tar}}}^{\pi}} \left[\int_{s'} |P_{\text{tar}}(s'|s,a) - P_{\text{src}}(s'|s,a)| \right],
 \end{aligned}$$

where the first equality holds from the telescoping lemma (Xu et al., 2018). Moreover, by the definition of total variance distance, we have

$$\begin{aligned}
 &\frac{\gamma \cdot r_{\max}}{(1-\gamma)^2} \mathbb{E}_{s,a \sim \rho_{\mathcal{M}_{\text{tar}}}^{\pi}} \left[\int_{s'} |P_{\text{tar}}(s'|s,a) - P_{\text{src}}(s'|s,a)| \right] \\
 &= \frac{2\gamma r_{\max}}{(1-\gamma)^2} \mathbb{E}_{s,a \sim \rho_{\mathcal{M}_{\text{tar}}}^{\pi}} [D_{\text{TV}}(P_{\text{tar}}(\cdot|s,a), P_{\text{src}}(\cdot|s,a))] \\
 &\leq \frac{2\gamma r_{\max}}{(1-\gamma)^2} \cdot \sup_{s,a} [D_{\text{TV}}(P_{\text{tar}}(\cdot|s,a), P_{\text{src}}(\cdot|s,a))].
 \end{aligned}$$

Combining the above two inequalities completes the proof. \square

Remark. Let $C_1 = \frac{2\gamma r_{\max}}{(1-\gamma)^2}$, which scales as $\mathcal{O}(\frac{1}{(1-\gamma)^2})$. This constant could be further reduced to $\mathcal{O}(\frac{1}{1-\gamma})$ to ensure a tighter performance bound, under the Lipschitz continuity assumption. Specifically, we introduce the following assumption and corollary.

Assumption B.1 (Lipschitz Continuity.). The learned V -function is K_V -Lipschitz, w.r.t. state s , i.e., $\forall s_1, s_2 \in \mathcal{S}$, $|V(s_1) - V(s_2)| \leq K_V \|s_1 - s_2\|$.

Corollary B.2 (Tighter Performance Bound.). *Under Assumption B.1, the performance difference of a policy π under \mathcal{M}_{src} and \mathcal{M}_{tar} admits a tighter bound as*

$$|J_{\mathcal{M}_{\text{src}}}(\pi) - J_{\mathcal{M}_{\text{tar}}}(\pi)| \leq C \cdot \sup_{s,a} [D_{TV}(P_{\text{src}}(\cdot|s,a), P_{\text{tar}}(\cdot|s,a))],$$

where $C = \frac{\gamma}{1-\gamma} \cdot K_V$.

Proof. The conclusion can be directly obtained by following the proof procedure of Theorem 4.5 of Ji et al. (2022). \square

B.2. Proof of Proposition 4.2

Proof. We first decompose the desired performance bound into four parts:

$$\begin{aligned} & |J_{\mathcal{M}_{\text{tar}}}(\hat{\pi}) - J_{\mathcal{M}_{\text{tar}}}(\pi_{\text{tar}}^*)| \\ &= |(J_{\mathcal{M}_{\text{src}}}(\hat{\pi}) - J_{\mathcal{M}_{\text{src}}}(\pi_{\text{insrc}}^*)) + (J_{\mathcal{M}_{\text{tar}}}(\hat{\pi}) - J_{\mathcal{M}_{\text{src}}}(\hat{\pi})) + (J_{\mathcal{M}_{\text{src}}}(\pi_{\text{src}}^*) - J_{\mathcal{M}_{\text{tar}}}(\pi_{\text{tar}}^*)) \\ &+ (J_{\mathcal{M}_{\text{src}}}(\pi_{\text{insrc}}^*) - J_{\mathcal{M}_{\text{src}}}(\pi_{\text{src}}^*))| \\ &\leq \underbrace{|J_{\mathcal{M}_{\text{src}}}(\hat{\pi}) - J_{\mathcal{M}_{\text{src}}}(\pi_{\text{insrc}}^*)|}_{\text{(I)}} + \underbrace{|J_{\mathcal{M}_{\text{tar}}}(\hat{\pi}) - J_{\mathcal{M}_{\text{src}}}(\hat{\pi})|}_{\text{(II)}} + \underbrace{|J_{\mathcal{M}_{\text{src}}}(\pi_{\text{src}}^*) - J_{\mathcal{M}_{\text{tar}}}(\pi_{\text{tar}}^*)|}_{\text{(III)}} \\ &+ \underbrace{|J_{\mathcal{M}_{\text{src}}}(\pi_{\text{insrc}}^*) - J_{\mathcal{M}_{\text{src}}}(\pi_{\text{src}}^*)|}_{\text{(IV)}}. \end{aligned}$$

Part (I) is exactly the desired term (a), i.e., the sub-optimality on the source domain. To get term (b), we need to bound parts (II) and (III), respectively.

We first bound part (II). By directly using Lemma 4.1, we have

$$\begin{aligned} \text{(II)} &:= |J_{\mathcal{M}_{\text{tar}}}(\hat{\pi}) - J_{\mathcal{M}_{\text{src}}}(\hat{\pi})| \\ &\leq \frac{2\gamma r_{\max}}{(1-\gamma)^2} \cdot \sup_{s,a} [D_{TV}(P_{\text{tar}}(\cdot|s,a), P_{\text{src}}(\cdot|s,a))]. \end{aligned}$$

Next, we bound part (III), i.e., the performance discrepancy between the optimal policy of two different MDPs.

For part (III), according to the definition of $J_{\mathcal{M}}(\hat{\pi})$, we have $J_{\mathcal{M}}(\hat{\pi}) = V_{\mathcal{M},h=0}^{\hat{\pi}}(s) := \mathbb{E}_{s \sim \rho_{\mathcal{M}}} [V_{\mathcal{M}}^{\hat{\pi}}(s)]$. To get the performance bound between two optimal policies in two MDPs, we can turn to analyze the optimal value difference of two MDPs at horizon 0 as

$$\text{(III)} := |V_{\mathcal{M}_{\text{src}},h=0}^*(s) - V_{\mathcal{M}_{\text{tar}},h=0}^*(s)|. \quad (7)$$

To analyze Equation 7, we first consider the value difference at step $h - 1$:

$$\begin{aligned}
 & V_{\text{src},h-1}^*(s) - V_{\text{tar},h-1}^*(s) \\
 &= \max_{a \in \mathcal{A}} \int_{s'} P_{\text{src}}(s'|s, a) (r(s, a) + \gamma V_{\text{src},h}^*(s')) - \max_{a \in \mathcal{A}} \int_{s'} P_{\text{tar}}(s'|s, a) (r(s, a) + \gamma V_{\text{tar},h}^*(s')) \\
 &= \int_{s'} P_{\text{src}}(s'|s, a_1) (r(s, a_1) + \gamma V_{\text{src},h}^*(s')) - \int_{s'} P_{\text{tar}}(s'|s, a_2) (r(s, a_2) + \gamma V_{\text{tar},h}^*(s')) \\
 &\leq \int_{s'} P_{\text{src}}(s'|s, a_1) (r(s, a_1) + \gamma V_{\text{src},h}^*(s')) - \int_{s'} P_{\text{tar}}(s'|s, a_1) (r(s, a_1) + \gamma V_{\text{tar},h}^*(s')) \\
 &= \int_{s'} (P_{\text{src}}(s'|s, a_1) - P_{\text{tar}}(s'|s, a_1)) r(s, a_1) + \gamma \int_{s'} (P_{\text{src}}(s'|s, a_1) V_{\text{src},h}^*(s') - P_{\text{tar}}(s'|s, a_1) V_{\text{tar},h}^*(s')) \\
 &\leq \max_{a \in \mathcal{A}} \int_{s'} (P_{\text{src}}(s'|s, a) - P_{\text{tar}}(s'|s, a)) r(s, a) + \max_{a \in \mathcal{A}} \left[\gamma \int_{s'} (P_{\text{src}}(s'|s, a) V_{\text{src},h}^*(s') - P_{\text{tar}}(s'|s, a) V_{\text{tar},h}^*(s')) \right],
 \end{aligned}$$

where in the second equality, we have $a_1 = \arg \max_{a \in \mathcal{A}} \int_{s'} P_{\text{src}}(s'|s, a) (r(s, a) + \gamma V_{\text{src},h}^*(s'))$, and $a_2 = \arg \max_{a \in \mathcal{A}} \int_{s'} P_{\text{tar}}(s'|s, a) (r(s, a) + \gamma V_{\text{tar},h}^*(s'))$. In addition, we have

$$\begin{aligned}
 & \max_{a \in \mathcal{A}} \int_{s'} (P_{\text{src}}(s'|s, a) - P_{\text{tar}}(s'|s, a)) r(s, a) \leq \max_{a \in \mathcal{A}} \int_{s'} |P_{\text{src}}(s'|s, a) - P_{\text{tar}}(s'|s, a)| \cdot r_{\max}, \\
 & \max_{a \in \mathcal{A}} \left[\gamma \int_{s'} (P_{\text{src}}(s'|s, a) V_{\text{src},h}^*(s') - P_{\text{tar}}(s'|s, a) V_{\text{tar},h}^*(s')) \right] \\
 & \leq \gamma \max_{a \in \mathcal{A}} \int_{s'} P_{\text{tar}}(s'|s, a) (V_{\text{src},h}^*(s') - V_{\text{tar},h}^*(s')) + \gamma \max_{a \in \mathcal{A}} \int_{s'} |P_{\text{src}}(s'|s, a) - P_{\text{tar}}(s'|s, a)| V_{\text{src},h}^*(s').
 \end{aligned}$$

Therefore, combining them together, we obtain

$$\begin{aligned}
 & V_{\text{src},h-1}^*(s) - V_{\text{tar},h-1}^*(s) \\
 & \leq \frac{2r_{\max}}{1-\gamma} \sup_{s,a} [D_{\text{TV}}(P_{\text{tar}}(\cdot|s, a), P_{\text{src}}(\cdot|s, a))] + \gamma \max_{s' \in \mathcal{S}} [V_{\text{src},h}^*(s') - V_{\text{tar},h}^*(s')].
 \end{aligned} \tag{8}$$

If we denote

$$a_h := \max_{s \in \mathcal{S}} [V_{\text{src},h}^*(s) - V_{\text{tar},h}^*(s)]$$

and

$$c := \frac{2r_{\max}}{1-\gamma} \sup_{s,a} [D_{\text{TV}}(P_{\text{tar}}(\cdot|s, a), P_{\text{src}}(\cdot|s, a))],$$

then Equation 8 can be simplified as

$$\begin{aligned}
 & a_{h-1} \leq c + \gamma a_h \\
 \Rightarrow & a_{h-1} - \frac{c}{1-\gamma} \leq \gamma \cdot \left(a_h - \frac{c}{1-\gamma} \right).
 \end{aligned} \tag{9}$$

Note that Equation 9 is a recursive expression. Repeating the process recursively, we can easily get

$$a_0 - \frac{c}{1-\gamma} \leq \gamma^H \left(a_H - \frac{c}{1-\gamma} \right), \tag{10}$$

where H denotes the maximum step of an episode¹. According to the definition of the state value, the value of the terminal state is 0, thus $a_H = 0$. Plugging $a_H = 0$ into Equation 10, we can get

$$V_{\text{src},0}^*(s) - V_{\text{tar},0}^*(s) \leq a_0 \leq c \cdot \frac{1-\gamma^H}{1-\gamma}.$$

¹We focus on the infinite-horizon setting, and H only serves as an intermediate variable for analysis.

If we set $H \rightarrow \infty$, we have

$$V_{\text{src},0}^*(s) - V_{\text{tar},0}^*(s) \leq \frac{2r_{\max}}{(1-\gamma)^2} \sup_{s,a} [D_{\text{TV}}(P_{\text{tar}}(\cdot|s,a), P_{\text{src}}(\cdot|s,a))].$$

Due to the interchangeability of \mathcal{M}_{src} and \mathcal{M}_{tar} , we also have

$$V_{\text{src},0}^*(s) - V_{\text{tar},0}^*(s) \geq -\frac{2r_{\max}}{(1-\gamma)^2} \sup_{s,a} [D_{\text{TV}}(P_{\text{tar}}(\cdot|s,a), P_{\text{src}}(\cdot|s,a))].$$

Therefore,

$$\begin{aligned} \text{(III)} &:= |V_{\mathcal{M}_{\text{src}},h=0}^*(s) - V_{\mathcal{M}_{\text{tar}},h=0}^*(s)| \\ &\leq \frac{2r_{\max}}{(1-\gamma)^2} \sup_{s,a} [D_{\text{TV}}(P_{\text{tar}}(\cdot|s,a), P_{\text{src}}(\cdot|s,a))]. \end{aligned}$$

Combining the bounds of terms (II) and (III), we get

$$\text{(II)} + \text{(III)} \leq C_2 \cdot \sup_{s,a} [D_{\text{TV}}(P_{\text{tar}}(\cdot|s,a), P_{\text{src}}(\cdot|s,a))],$$

where $C_2 = \frac{(2\gamma+2)r_{\max}}{(1-\gamma)^2}$.

For the term (IV), its value is exactly ϵ_{src}^* by the definition of ϵ_{src}^* . This concludes the proof. \square

Remark. Similar to Lemma 4.1, C_2 could be further reduced to $C = \frac{2\gamma}{1-\gamma} \cdot K_V$ under the Lipschitz continuity assumption.

B.3. Proof of Proposition 5.1

Proof. We first divide the sub-optimality on the source domain into two terms:

$$J_{\mathcal{M}_{\text{src}}}(\hat{\pi}) - J_{\mathcal{M}_{\text{src}}}(\pi_{\text{insrc}}^*) = \underbrace{J_{\mathcal{M}_{\text{src}}}(\mu) - J_{\mathcal{M}_{\text{src}}}(\pi_{\text{insrc}}^*)}_{\text{(i)}} + \underbrace{J_{\mathcal{M}_{\text{src}}}(\hat{\pi}) - J_{\mathcal{M}_{\text{src}}}(\mu)}_{\text{(ii)}}.$$

We first focus on term (i). By using performance difference lemma (Kakade & Langford, 2002), the return difference between π and π_{insrc}^* in \mathcal{M}_{src} gives:

$$\begin{aligned} J_{\mathcal{M}_{\text{src}}}(\mu) - J_{\mathcal{M}_{\text{src}}}(\pi_{\text{insrc}}^*) &= \int_s d_\mu(s) \int_a [\mu(a|s) A_{\pi_{\text{insrc}}^*}(s,a)] \\ &= \mathbb{E}_{s \sim d_\mu(\cdot), a \sim \mu(\cdot|s)} [A_{\pi_{\text{insrc}}^*}(s,a)]. \end{aligned} \quad (11)$$

Thus we get the first term in the desired bound. Then we turn to derive the second term.

Based on the Corollary 1 in (Achiam et al., 2017), we have

$$J_{\mathcal{M}_{\text{src}}}(\hat{\pi}) - J_{\mathcal{M}_{\text{src}}}(\mu) \geq \int_s d_\mu(s) \int_a [\hat{\pi}(a|s) A_\mu(s,a)] - \frac{2\gamma\epsilon_\mu^{\hat{\pi}}}{(1-\gamma)^2} D_{\text{TV}}^{d_\mu}(\hat{\pi}, \mu),$$

where $\epsilon_\mu^{\hat{\pi}} = \max_s [\mathbb{E}_{a \sim \hat{\pi}} A_\mu(s,a)]$, and $D_{\text{TV}}^{d_\mu}(\hat{\pi}, \mu) = \frac{1}{2} \int_s d_\mu(s) \int_a |\hat{\pi}(a|s) - \mu(a|s)|$ is the total variance distance between $\hat{\pi}$ and μ over the distribution d_μ .

Note that under the assumption that for all (s,a) , then $(\hat{\pi}(a|s) - \mu(a|s)) A_\mu(s,a) \geq 0$, we have

$$\begin{aligned} &\int_s d_\mu(s) \int_a [\hat{\pi}(a|s) A_\mu(s,a)] \\ &= \int_s d_\mu(s) \int_a [(\hat{\pi}(a|s) - \mu(a|s)) A_\mu(s,a)] + \int_s d_\mu(s) \int_a [\mu(a|s) A_\mu(s,a)] \\ &\geq 0 + 0 \\ &= 0. \end{aligned} \quad (12)$$

Equation 12 uses the fact that $\int_a [\mu(a|s)A_\mu(s, a)] = 0$. An important fact is that π is updated via offline RL (such as IQL), which imposes implicit or explicit policy constraints on π . We follow the constraints in IQL and assume

$$\max_s (\text{KL}(\mu(\cdot|s), \hat{\pi}(\cdot|s)), \text{KL}(\hat{\pi}(\cdot|s), \mu(\cdot|s))) \leq \epsilon.$$

Then we have

$$\begin{aligned} J_{\mathcal{M}_{\text{src}}}(\hat{\pi}) - J_{\mathcal{M}_{\text{src}}}(\mu) &\geq 0 - \frac{2\gamma\epsilon_\mu^{\hat{\pi}}}{(1-\gamma)^2} D_{TV}^{d_\mu}(\hat{\pi}, \mu) \\ &\geq -\frac{2\gamma\epsilon_\mu^{\hat{\pi}}}{(1-\gamma)^2} \int_s d_\mu(s) \min\left(\sqrt{\text{KL}(\mu(\cdot|s), \hat{\pi}(\cdot|s))}, \sqrt{\text{KL}(\hat{\pi}(\cdot|s), \mu(\cdot|s))}\right) \\ &\geq -\frac{2\gamma\epsilon_\mu^{\hat{\pi}}}{(1-\gamma)^2} \int_s d_\mu(s) \max\left(\sqrt{\text{KL}(\mu(\cdot|s), \hat{\pi}(\cdot|s))}, \sqrt{\text{KL}(\hat{\pi}(\cdot|s), \mu(\cdot|s))}\right) \\ &\geq -\frac{2\gamma\epsilon_\mu^{\hat{\pi}}}{(1-\gamma)^2} \cdot \sqrt{\epsilon}. \end{aligned}$$

The second inequality results from Pinsker's inequality (Csiszár & Körner, 2011). Hence, we conclude that for policy $\hat{\pi}$ learned on the source domain via IQL, it induces a safe policy improvement:

$$J_{\mathcal{M}_{\text{src}}}(\hat{\pi}) - J_{\mathcal{M}_{\text{src}}}(\mu) \geq -\mathcal{O}\left(\frac{1}{(1-\gamma)^2}\right). \quad (13)$$

By combining the result of Equation 11 and Equation 13, we have

$$J_{\mathcal{M}_{\text{src}}}(\hat{\pi}) - J_{\mathcal{M}_{\text{src}}}(\pi_{\text{insrc}}^*) \geq \mathbb{E}_{s \sim \rho_\mu(\cdot), a \sim \mu(\cdot|s)} [A_{\pi_{\text{insrc}}^*}(s, a)] - \mathcal{O}\left(\frac{1}{(1-\gamma)^2}\right). \quad (14)$$

Since for a policy $\hat{\pi}$ learned using an in-sample offline RL algorithm (e.g., IQL), $J_{\mathcal{M}_{\text{src}}}(\hat{\pi}) - J_{\mathcal{M}_{\text{src}}}(\pi_{\text{insrc}}^*) \leq 0$ holds. Therefore we have

$$|J_{\mathcal{M}_{\text{src}}}(\hat{\pi}) - J_{\mathcal{M}_{\text{src}}}(\pi_{\text{insrc}}^*)| \leq -\mathbb{E}_{s \sim \rho_\mu(\cdot), a \sim \mu(\cdot|s)} [A_{\pi_{\text{insrc}}^*}(s, a)] + \mathcal{O}\left(\frac{1}{(1-\gamma)^2}\right). \quad (15)$$

Then we conclude the proof. \square

B.4. Proof of Proposition 5.2

Proof. We first decompose the objective into two terms:

$$\begin{aligned} \mathbb{E}_{s \sim \rho_\mu(\cdot), a \sim \mu(\cdot|s)} [\hat{A}_{\text{pre}}(s, a) - A_{\pi_{\text{insrc}}^*}(s, a)] &= \mathbb{E}_{s \sim \rho_\mu(\cdot), a \sim \mu(\cdot|s)} [A_{\text{pre}}(s, a) - A_{\pi_{\text{insrc}}^*}(s, a)] \\ &\quad + \mathbb{E}_{s \sim \rho_\mu(\cdot), a \sim \mu(\cdot|s)} [\hat{A}_{\text{pre}}(s, a) - A_{\text{pre}}(s, a)]. \end{aligned}$$

For the first term, using the performance difference lemma (Kakade & Langford, 2002), we have

$$J_{\mathcal{M}_{\text{src}}}(\mu) - J_{\mathcal{M}_{\text{src}}}(\pi_{\text{pre}}) = \mathbb{E}_{s \sim \rho_\mu(\cdot), a \sim \mu(\cdot|s)} [A_{\pi_{\text{pre}}}(s, a)], \quad (16)$$

$$J_{\mathcal{M}_{\text{src}}}(\mu) - J_{\mathcal{M}_{\text{src}}}(\pi_{\text{insrc}}^*) = \mathbb{E}_{s \sim \rho_\mu(\cdot), a \sim \mu(\cdot|s)} [A_{\pi_{\text{insrc}}^*}(s, a)]. \quad (17)$$

By subtracting Equation 16 with Equation 17, we can get $\Delta J_{\mathcal{M}_{\text{src}}}(\pi_{\text{insrc}}^*, \pi_{\text{pre}})$. The second term is exactly $\mathbb{E}_{s \sim \rho_\mu(\cdot), a \sim \mu(\cdot|s)} [\Delta(s, a)]$. This concludes the proof. \square

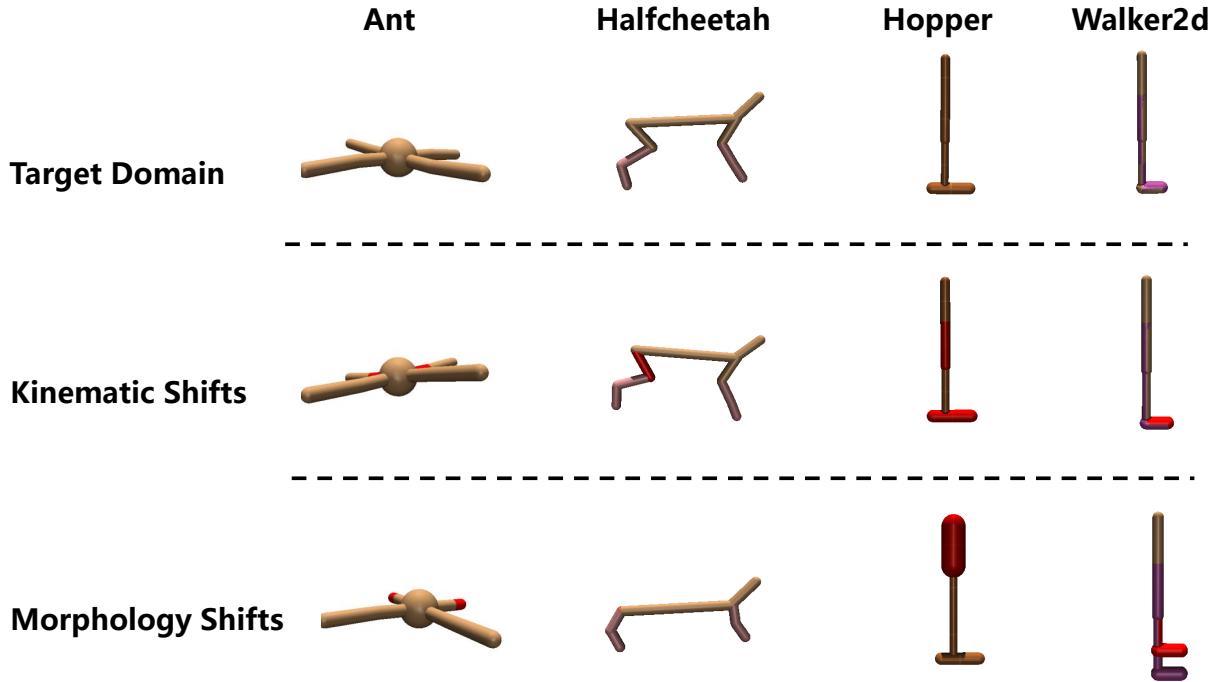


Figure 4. Visualization of the target domains and source domains with kinematic shifts and morphology shifts, across four tasks (ant, halfcheetah, hopper, walker2d).

C. Environment Setting

In this section, we supplement the detailed environmental settings we adopt in our experiments, including the information of source and target domain datasets, and the code-level realization of kinematic shifts and morphology shifts, etc.

C.1. Datasets and Metrics

Target domain datasets. In the cross-domain offline RL setting, the target domain datasets should be collected in the target environment, and only limited target domain data is available. To this end, we directly sample a proportion of data from widely used D4RL (Fu et al., 2020) MuJoCo datasets as the target domain datasets. In D4RL, the MuJoCo datasets are collected with an online SAC (Haarnoja et al., 2018) agent in the environments of Gym (Brockman et al., 2016) simulated by MuJoCo engine (Todorov et al., 2012). We adopt four tasks in our experiments: halfcheetah-v2, hopper-v2, walker2d-v2, ant-v3, and consider five dataset qualities for each task: random, medium, medium-replay, medium-expert, expert. In D4RL, the **random** datasets are collected with a randomly initialized policy. The **medium** datasets contain 1M samples collected from an early-stopped SAC policy. The **medium-replay** datasets record the replay buffer of an SAC agent trained up to the performance of the medium-level agent. The **medium-expert** datasets are a mixture of medium data and expert data at a 50-50 ratio. The **expert** datasets contain 1M samples logged from an expert policy. To construct target domain datasets with different sizes, we sample different numbers of data from the D4RL datasets. In Section 6.1, we sample 10% data from each D4RL dataset, and in Section E.2, we only sample 5,000 transitions for each dataset to simulate a very limited target data setting.

Source domain datasets. To fully examine the effectiveness of our method, we design two kinds of dynamics shift scenarios based on four widely used MuJoCo tasks: halfcheetah-v2, hopper-v2, walker2d-v2, ant-v3. The types of dynamics shift we implement include kinematic shift and morphology shift. The kinematic shift means that some joints of the simulated robot are broken and fail to rotate. The morphology shift indicates that the morphology of the simulated robot in the two domains is different. We show the visualization results of the simulated robot in the source domain and target domain in Figure 4. And the code-level modifications for realizing the dynamics shifts are deferred to the following subsections.

To construct source domain datasets, we follow a similar data-collecting procedure as in D4RL and collect the datasets in the revised environments. We train an online SAC agent within the environments with different kinds of dynamics shifts for 1M steps, and we log the checkpoints of the policy with different training steps and use them to roll out trajectories. The **random** datasets are generated by directly sampling the action space. The **medium** datasets are gathered with the logged policy that exhibits about 1/2 performance of the expert policy. The **medium-replay** datasets consist of the replay buffer of the medium-level agent. We sample 50% data from the medium datasets and 50% data from the expert datasets, then we mix the sampled data and construct the **medium-expert** datasets. The **expert** datasets are gathered using the last policy checkpoint.

Metrics. The metric we use for evaluating the performance of the offline policy in the target domain is the `normalized score (NS)` in D4RL. It is computed as follows:

$$\text{NS} = \frac{J_{\pi} - J_{\text{random}}}{J_{\text{expert}} - J_{\text{random}}} \times 100\%,$$

where J is the return acquired by the agent in the target domain, J_{random} and J_{expert} are the returns obtained by the random policy and the expert policy in the target domain, respectively.

C.2. Kinematic Shift Tasks

To simulate the kinematic shifts between the source domain and target domain, we modify the `xml` files of the original environments. Specifically, we change the rotation angle of some joints of the simulated robot for different tasks:

halfcheetah-kinematic: The rotation angle of the joint on the thigh of the robot’s back leg is modified from $[-0.52, 1.05]$ to $[-0.0052, 0.0105]$.

```
# broken back thigh joint
<joint axis="0 1 0" damping="6" name="bthigh" pos="0 0 0" range="-0.0052 0.0105"
  stiffness="240" type="hinge"/>
```

hopper-kinematic: The rotation angle of the head joint is modified from $[-150, 0]$ to $[-0.15, 0]$ and the rotation angle of the foot joint is modified from $[-45, 45]$ to $[-18, 18]$.

```
# broken head joint
<joint axis="0 -1 0" name="thigh_joint" pos="0 0 1.05" range="-0.15 0" type="
  hinge"/>
# broken foot joint
<joint axis="0 -1 0" name="foot_joint" pos="0 0 0.1" range="-18 18" type="hinge"
  />
```

walker2d-kinematic: The rotation angle of the right foot joint is modified from $[-45, 45]$ to $[-0.45, 0.45]$.

```
# broken right foot joint
<joint axis="0 -1 0" name="foot_joint" pos="0 0 0.1" range="-0.45 0.45" type="
  hinge"/>
```

ant-kinematic: The rotation angles of the joints on the hip of two front legs are modified from $[-30, 30]$ to $[-0.3, 0.3]$.

```
# broken hip joints of front legs
<joint axis="0 0 1" name="hip_1" pos="0.0 0.0 0.0" range="-0.3 0.3" type="hinge"
  />
<joint axis="0 0 1" name="hip_2" pos="0.0 0.0 0.0" range="-0.3 0.3" type="hinge"
  />
```

C.3. Morphology Shift Tasks

Akin to the kinematic shifts, we modify the morphology of the simulated robot to simulate the morphology shifts:

halfcheetah-morph: The sizes of the back thigh and the forward thigh are modified.

```
# back thigh
<geom fromto="0 0 0 -0.0001 0 -0.0001" name="bthigh" size="0.046" type="capsule"
  />
<body name="bshin" pos="-0.0001 0 -0.0001">
# front thigh
<geom fromto="0 0 0 0.0001 0 0.0001" name="fthigh" size="0.046" type="capsule"/>
<body name="fshin" pos="0.0001 0 0.0001">
```

hopper-morph: The head size of the robot is modified.

```
# head size
<geom friction="0.9" fromto="0 0 1.45 0 0 1.05" name="torso_geom" size="0.125"
  type="capsule"/>
```

walker2d-morph: The thigh on the right leg of the robot is modified.

```
# right leg
<body name="thigh" pos="0 0 1.05">
<joint axis="0 -1 0" name="thigh_joint" pos="0 0 1.05" range="-150 0" type="hinge"
  />
<geom friction="0.9" fromto="0 0 1.05 0 0 1.045" name="thigh_geom" size="0.05"
  type="capsule"/>
<body name="leg" pos="0 0 0.35">
  <joint axis="0 -1 0" name="leg_joint" pos="0 0 1.045" range="-150 0" type="
    hinge"/>
  <geom friction="0.9" fromto="0 0 1.045 0 0 0.3" name="leg_geom" size="0.04"
    type="capsule"/>
  <body name="foot" pos="0.2 0 0">
    <joint axis="0 -1 0" name="foot_joint" pos="0 0 0.3" range="-45 45" type="
      hinge"/>
    <geom friction="0.9" fromto="-0.0 0 0.3 0.2 0 0.3" name="foot_geom" size="0.06"
      type="capsule"/>
  </body>
</body>
</body>
</body>
```

ant-morph: The size of the robot's two front legs is reduced.

```
# front leg 1
<geom fromto="0.0 0.0 0.0 0.1 0.1 0.0" name="left_ankle_geom" size="0.08" type="
  capsule"/>
# front leg 2
<geom fromto="0.0 0.0 0.0 -0.1 0.1 0.0" name="right_ankle_geom" size="0.08" type="
  capsule"/>
```

D. Implementation Details

In this section, we provide more details about the implementation of the baseline methods and our method. We also list the hyperparameter setup for all methods.

D.1. Baselines

IQL: IQL (Kostrikov et al., 2021) is an off-the-shelf offline RL algorithm that learns the policy in an *in-sample manner*, which means no OOD samples that lie outside of the offline datasets are required during training. In the cross-domain offline

setting, we follow the algorithm procedure but draw samples from both the source domain dataset and the target domain dataset. IQL trains the state value function via expectile regression:

$$\mathcal{L}_V = \mathbb{E}_{(s,a) \sim \mathcal{D}_{\text{src}} \cup \mathcal{D}_{\text{tar}}} [L_2^\tau(Q_{\theta'}(s, a) - V_\psi(s))]$$

where $L_2^\tau(u) = |\tau - \mathbb{I}(u < 0)| u^2$, $\mathbb{I}(\cdot)$ is the indicator function, and θ' is the target network parameter. With such expectile regression, an in-sample optimal value function can be learned. Then the state-action value function is updated by:

$$\mathcal{L}_Q = \mathbb{E}_{(s,a,r,s') \sim \mathcal{D}_{\text{src}} \cup \mathcal{D}_{\text{tar}}} [(r(s, a) + \gamma V_\psi(s') - Q_\theta(s, a))^2]$$

Then the advantage value is calculated as $A(s, a) = Q(s, a) - V(s, a)$ and the policy is extracted by advantage weighted behavior cloning:

$$\mathcal{L}_\pi = -\mathbb{E}_{(s,a) \sim \mathcal{D}_{\text{src}} \cup \mathcal{D}_{\text{tar}}} [\exp(\beta \times A(s, a)) \log \pi_\phi(a|s)],$$

where β is the inverse temperature coefficient. We implement IQL by following its official codebase².

BOSA: BOSA (Liu et al., 2024a) defines the issues of the state-action OOD problem and the dynamics OOD problem in cross-domain offline RL, and proposes two support constraints to tackle the issues. To be specific, BOSA handles the OOD state-action problem by supported policy optimization, and mitigates the OOD dynamics problem by supported value optimization. BOSA updates the critic by supported value optimization:

$$\mathcal{L}_Q = \mathbb{E}_{(s,a) \sim \mathcal{D}_{\text{src}}} [Q_{\theta_i}(s, a)] + \mathbb{E}_{(s,a,r,s') \sim \mathcal{D}_{\text{src}} \cup \mathcal{D}_{\text{tar}}, a' \sim \pi_\phi(s')} [\mathbb{I}(\hat{P}_{\text{tar}}(s'|s, a) > \epsilon)(Q_{\theta_i}(s, a) - y)^2],$$

where $\mathbb{I}(\cdot)$ is the indicator function, and $\hat{P}_{\text{tar}}(s'|s, a)$ is the target domain transition dynamics estimated via maximum likelihood estimation, and ϵ is the threshold coefficient. The policy in BOSA is updated by supported policy optimization:

$$\mathcal{L}_\pi = \mathbb{E}_{s \sim \mathcal{D}_{\text{src}} \cup \mathcal{D}_{\text{tar}}, a \sim \pi_\phi(s)} [Q_{\theta_i}(s, a)], \quad \text{s.t. } \mathbb{E}_{s \sim \mathcal{D}_{\text{src}} \cup \mathcal{D}_{\text{tar}}} [\hat{\pi}_{\text{mix}}(\pi_\phi(s) | s)] > \epsilon',$$

where ϵ' is the threshold coefficient, and $\hat{\pi}_{\text{mix}}(\cdot|s)$ is the empirical behavior policy of the mixed datasets $\mathcal{D}_{\text{src}} \cup \mathcal{D}_{\text{tar}}$ learned with CVAE (Kingma et al., 2013). We do not find the official implementation for BOSA, so we use the codebase³ in ODRL benchmark (Lyu et al., 2024b), which provides high-quality implementations for various off-dynamics RL algorithms.

DARA. DARA (Liu et al., 2022) leverages dynamics-aware reward modification to fulfill dynamics adaptation and is the offline version of DARC (Eysenbach et al., 2020). DARA trains two domain classifiers $q_{\theta_{SAS}}(\text{target}|s_t, a_t, s_{t+1})$ and $q_{\theta_{SA}}(\text{target}|s_t, a_t)$ as follows.

$$\begin{aligned} \mathcal{L}_{\theta_{SAS}} &= \mathbb{E}_{\mathcal{D}_{\text{tar}}} [\log q_{\theta_{SAS}}(\text{target}|s_t, a_t, s_{t+1})] + \mathbb{E}_{\mathcal{D}_{\text{src}}} [\log(1 - q_{\theta_{SAS}}(\text{target}|s_t, a_t, s_{t+1}))], \\ \mathcal{L}_{\theta_{SA}} &= \mathbb{E}_{\mathcal{D}_{\text{tar}}} [\log q_{\theta_{SA}}(\text{target}|s_t, a_t)] + \mathbb{E}_{\mathcal{D}_{\text{src}}} [\log(1 - q_{\theta_{SA}}(\text{target}|s_t, a_t))], \end{aligned}$$

The two domain classifiers are used to estimate the dynamics gap $\log \frac{P_{\mathcal{M}_{\text{tar}}(s_{t+1}|s_t, a_t)}}{P_{\mathcal{M}_{\text{src}}(s_{t+1}|s_t, a_t)}}$ between the source domain and the target domain. Then the estimated dynamics gap is used as a penalty to the source domain rewards:

$$\hat{r}_{\text{DARA}} = r - \lambda \times \delta_r, \quad \delta_r(s_t, a_t) = -\log \frac{q_{\theta_{SAS}}(\text{target}|s_t, a_t, s_{t+1})q_{\theta_{SA}}(\text{source}|s_t, a_t)}{q_{\theta_{SAS}}(\text{source}|s_t, a_t, s_{t+1})q_{\theta_{SA}}(\text{target}|s_t, a_t)},$$

where λ controls the intensity of the reward penalty. We use the re-implementation in ODRL for DARA. λ is set to 0.1, and the reward penalty is clipped within $[-10, 10]$ for training stability.

IGDF. IGDF (Wen et al., 2024) estimates the domain gap between the source domain and the target domain with contrastive representation learning, and employs data filtering to share source domain samples with a smaller dynamics gap for training. IGDF trains a score function $h(\cdot)$ using $(s, a, s'_{\text{tar}}) \sim \mathcal{D}_{\text{tar}}$ as the positive samples, and transitions (s, a, s'_{src}) as the negative samples, where $(s, a) \sim \mathcal{D}_{\text{tar}}$ and $s'_{\text{src}} \sim \mathcal{D}_{\text{src}}$. $h(\cdot)$ is trained with the contrastive learning objective:

$$\mathcal{L} = -\mathbb{E}_{(s,a,s'_{\text{tar}})} \mathbb{E}_{s'_{\text{src}}} \left[\log \frac{h(s, a, s'_{\text{tar}})}{\sum_{s' \in s'_{\text{tar}} \cup s'_{\text{src}}} h(s, a, s')} \right]. \quad (18)$$

²https://github.com/ikostrikov/implicit_q_learning.git

³<https://github.com/OffDynamicsRL/off-dynamics-rl.git>

For the construction of the score function, IGDF adopts two networks $\phi(s, a)$ and $\psi(s')$ to learn the representations of state-action and state, respectively. The score function is expressed as a linear parameterization of $\phi(s, a)$ and $\psi(s')$:

$$h(s, a, s') = \exp(\phi(s, a)^T \psi(s')).$$

Based on the learned score function, IGDF proposes to selectively share source domain data for training value functions:

$$\mathcal{L}_Q = \frac{1}{2} \mathbb{E}_{\mathcal{D}_{\text{tar}}} [(Q_\theta - \mathcal{T}Q_\theta)^2] + \frac{1}{2} \alpha \cdot h(s, a, s') \mathbb{E}_{(s, a, s') \sim \mathcal{D}_{\text{src}}} [\mathbb{I}(h(s, a, s') > h_{\xi\%}) (Q_\theta - \mathcal{T}Q_\theta)^2],$$

where $\mathbb{I}(\cdot)$ is the indicator function, α is the weighting coefficient, ξ is the data selection ratio. We implement IGDF by following its official codebase⁴.

OTDF. OTDF (Lyu et al., 2025) depicts the distance between the source domain data and target domain data by computing the Wasserstein distance (Peyré et al., 2019):

$$\mathcal{W}(u, u') = \min_{\mu \in M} \sum_{t=1}^{|\mathcal{D}_{\text{src}}|} \sum_{t'=1}^{|\mathcal{D}_{\text{tar}}|} C(u_t, u'_{t'}) \cdot \mu_{t,t'}, \quad (19)$$

where $u = s_{\text{src}} \oplus a_{\text{src}} \oplus s'_{\text{src}}$, $u' = s_{\text{tar}} \oplus a_{\text{tar}} \oplus s'_{\text{tar}}$, C is the cost function and M is the coupling matrices. After solving Equation 19 for μ^* , the OTDF determines the deviation between a source domain dataset and the target domain dataset via:

$$d(u_t) = - \sum_{t'=1}^{|\mathcal{D}_{\text{tar}}|} C(u_t, u'_{t'}) \mu_{t,t'}^*, \quad u_t = (s_{\text{src}}^t, a_{\text{src}}^t, (s'_{\text{src}})^t) \sim \mathcal{D}_{\text{src}}.$$

Then the critic is updated by

$$\mathcal{L}_Q = \mathbb{E}_{\mathcal{D}_{\text{tar}}} [(Q_\theta - \mathcal{T}Q_\theta)^2] + \mathbb{E}_{(s, a, s') \sim \mathcal{D}_{\text{src}}} [\exp(\alpha \times d) \mathbb{I}(d > d_{\%}) (Q_\theta - \mathcal{T}Q_\theta)^2].$$

Besides, OTDF includes an extra policy regularization term that encourages the policy to be close to the support region of the target dataset:

$$\widehat{\mathcal{L}}_\pi = \mathcal{L}_\pi - \beta \times \mathbb{E}_{s \sim \mathcal{D}_{\text{src}} \cup \mathcal{D}_{\text{tar}}} \log \pi_{\text{tar}}^b(\pi(\cdot|s)|s),$$

where \mathcal{L}_π is the original policy optimization objective and β is the weight coefficient. We run the official code⁵ for OTDF in our experiments.

D.2. More Details of Motivation Example

In this section, we supplement with more details for our motivation example in Section 3.

We provide the visualization results of the random-expert mixed source domain dataset in Figure 5 (a). We further conduct an experiment to demonstrate the necessity of dynamics- and value-aligned data filtering. Instead of using $h(s, a, s')$ or $g(s, a, s')$ as the indicator like IGDF and DVDF, we directly use $A_{\text{pre}}(s, a)$ for data filtering, which means we select source domain data with a smaller value misalignment, disregarding dynamics misalignment. We term this modified algorithm version as Value-IGDF. We visualize the data filtering results (data selection ratio ξ is 25%) in Figure 5 (b), which indicates that the selected samples are predominantly expert samples, despite the dynamics shifts. We evaluate the performance of IGDF, Value-IGDF, and DVDF on the source domain and present the results in Figure 5 (c). We can see that while Value-IGDF outperforms IGDF, it still lags behind DVDF, highlighting the necessity of jointly considering dynamics and value alignment.

D.3. Algorithmic Details of DVDF

As a plug-in module, DVDF can be seamlessly integrated into various cross-domain offline RL algorithms, such as IGDF and OTDF. In this section, we present more details about the combination of DVDF with IGDF (tagged DVDF-IGDF) and OTDF (namely DVDF-OTDF), and summarize the pseudocodes of DVDF-IGDF and DVDF-OTDF.

⁴<https://github.com/BattleWen/IGDF.git>

⁵<https://github.com/dmksjfl/OTDF.git>

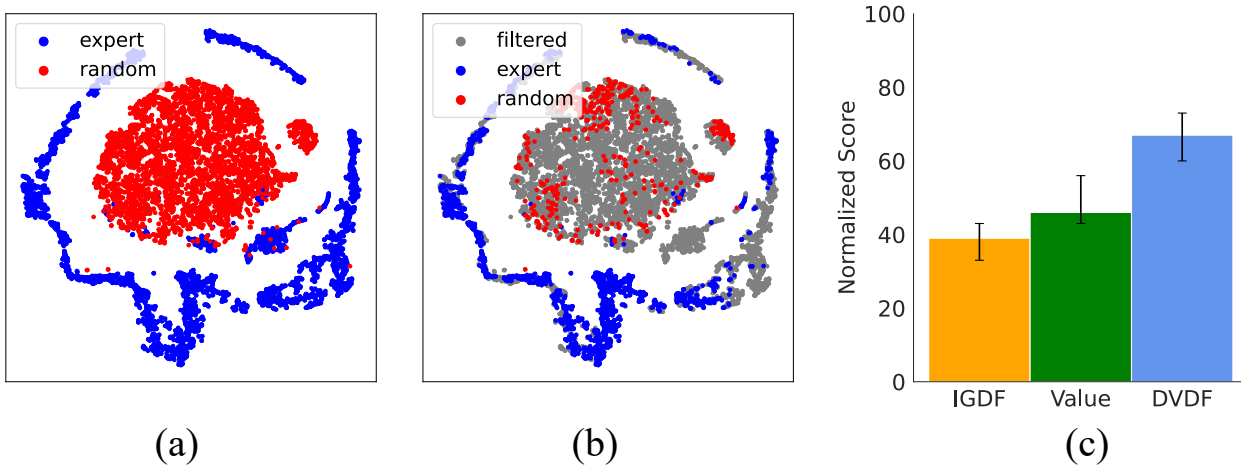


Figure 5. (a) Visualization of source domain data. (b) Source domain data filtering visualization of Value-IGDF. (c) Performance comparison between IGDF, Value-IGDF and DVDF.

For DVDF-IGDF, the new score function $g(\cdot)$ incorporates the vanilla score function $h(\cdot)$ and the pre-trained advantage function $A_{\text{pre}}(\cdot)$. During training, only $h(\cdot)$ is updated and $A_{\text{pre}}(\cdot)$ remains frozen. We leverage $g(\cdot)$ for data filtering, and the other procedures of DVDF-IGDF remain identical to those of IGDF. The detailed pseudocode of DVDF-IGDF is presented in Algorithm 1. The blue texts mark the different algorithm procedure from the original IGDF.

For DVDF-OTDF, other than $A_{\text{pre}}(\cdot)$, the optimal coupling μ^* also needs to be computed before the policy training process begins. We choose cosine distance as the cost function and utilize OTT-JAX library (Cuturi et al., 2022) for solving the OT problem. Note that DVDF only plays a part in the procedure of data filtering, and the remaining process of training remains the same as that in OTDF. We summarize the pseudocode of DVDF-OTDF in Algorithm 2. The blue lines highlight the different procedure from the vanilla OTDF.

D.4. Hyperparameter Setup

We present the main hyperparameter setup in our experiments for all the methods we use in Table 2.

E. Wider Experimental Results

E.1. Results under Morphology Shifts

In Section 6.1, we give the evaluation results of our methods with different sizes of target domain datasets under kinematic shifts. In this section, we supplement with more evaluation results under morphology shifts, with other experimental settings identical to Section 6.1.

Table 3 presents the comparison results using 10% data of the D4RL datasets as the target domain data. The results clearly show that DVDF enhances the performance of the base algorithms. Specifically, DVDF-IGDF achieves the highest total score among all the methods, outperforming IGDF by **15.4%** (1039.0 to 1198.7) and performing better in **16** out of 20 tasks, while DVDF-OTDF improves OTDF by **11.0%** (1042.1 to 1156.3) and excels in **14** out of 20 tasks.

E.2. Extended Results with Extremely Limited Target Data

In this section, we consider a more challenging setting compared with Section 6.1 following (Lyu et al., 2025; 2024b), where only extremely limited target domain data (around 5,000 transitions) are available. This setting reflects real-world scenarios, such as nuclear power plant control, where accessing more target domain data is often impractical. Typical offline RL will fail under such extreme data scarcity, making the proper utilization of source domain data much more crucial.

Tasks and Datasets. The tasks and types of dynamics shifts are identical to those in Section 6.1. The only distinction lies in the target domain datasets, which now consist of only 5,000 transitions sampled from the D4RL datasets, instead of the 10% subset used in Section 6.1.

Algorithm 1 DVDF-IGDF

- 1: **Require:** Source domain offline dataset \mathcal{D}_{src} , target domain offline dataset \mathcal{D}_{tar} , mixed offline dataset \mathcal{D}_{mix}
 - 2: **Initialization:** Policy network π_η , value network V_β , target Q network Q_θ , encoder networks $\phi(s, a)$, $\psi(s')$, data selection ratio ξ , batch size B , importance coefficient α , alignment tradeoff coefficient λ
 - 3: **// Pre-train the advantage function**
 - 4: Pre-train an SQL agent on \mathcal{D}_{src} , obtain $\hat{A}_{\text{pre}}(\cdot)$ and normalize $\hat{A}_{\text{pre}}(\cdot)$
 - 5: **// Contrastive Representation Learning**
 - 6: Train $h(s, a, s')$ via contrastive representation learning by Equation 18, obtain the score function $\omega(s, a, s') = \lambda \cdot h(s, a, s') + (1 - \lambda) \cdot \hat{A}_{\text{pre}}(s, a)$
 - 7: **// TD Learning**
 - 8: **for** each gradient step **do**
 - 9: Sample $b_{\text{src}} := \{(s, a, r, s')\}$ from \mathcal{D}_{src}
 - 10: Sample $b_{\text{tar}} := \{(s, a, r, s')\}$ from \mathcal{D}_{tar}
 - 11: Sample the top- ξ samples from b_{src} ranked by $g(s_{\text{src}}, a_{\text{src}}, s'_{\text{src}})$
 - 12: Compute weights $\omega(s, a, s')$ following:
 - 13: $\omega(s, a, s') = \mathbb{I}(g(s, a, s') \geq g_{\xi\%})$
 - 14: **// Optimize the V_β function**
 - 15: Compute loss \mathcal{L}_V :
 - 16: $\mathcal{L}_V = \mathbb{E}_{(s,a) \sim \mathcal{D}_{\text{src}} \cup \mathcal{D}_{\text{tar}}} [L_2^T(Q_\theta(s, a) - V_\beta(s))]$
 - 17: Update V_β using \mathcal{L}_V
 - 18: **// Optimize the Q_θ function**
 - 19: Compute loss \mathcal{L}_Q :
 - 20: $\mathcal{L}_Q = \frac{1}{2} \cdot \mathbb{E}_{(s,a,r,s') \sim \mathcal{D}_{\text{tar}}} [(Q_\theta(s, a) - (r + \gamma V_\beta(s')))^2]$
 - 21: $+ \frac{1}{2} \cdot \mathbb{E}_{(s,a,r,s') \sim \mathcal{D}_{\text{src}}} [\omega(s, a, s') g(s, a, s') (Q_\theta(s, a) - (r + \gamma V_\beta(s')))^2]$
 - 22: Update Q_θ using \mathcal{L}_Q
 - 23: **// Update target network**
 - 24: Update target network parameters: $\theta' \leftarrow (1 - \mu)\theta + \mu\theta'$
 - 25: **// Policy Extraction (AWR)**
 - 26: Compute advantage $A(s, a) = Q_\theta(s, a) - V_\beta(s)$
 - 27: Optimize policy network π_η using advantage-weighted regression (AWR):
 - 28: $\mathcal{L}_\pi = \mathbb{E}_{(s,a) \sim \mathcal{D}_{\text{src}} \cup \mathcal{D}_{\text{tar}}} [\exp(\alpha A(s, a)) \log \pi_\eta(a|s)]$
 - 29: **end for**
-

Algorithm 2 DVDF-OTDF

- 1: **Input:** Source domain dataset \mathcal{D}_{src} , target domain dataset \mathcal{D}_{tar} , batch size N , data selection ratio ξ , alignment tradeoff coefficient λ
 - 2: Initialize policy network π_ϕ , value networks V_ψ , Q_θ , target Q function $Q_{\theta'}$, the cost function C , policy coefficients β , number of sampled latent variables M , target update rate η
 - 3: **// Pre-train the advantage function**
 - 4: Pre-train an SQL agent on \mathcal{D}_{src} , obtain $\hat{A}_{\text{pre}}(\cdot)$ and normalize $\hat{A}_{\text{pre}}(\cdot)$
 - 5: **// Solve the OT problem**
 - 6: Compute the optimal alignment between \mathcal{D}_{src} and \mathcal{D}_{tar} with Equation 4
 - 7: Compute deviations $\{d_v\}_{v=1}^{|\mathcal{D}_{\text{src}}|}$ between the source domain data and \mathcal{D}_{tar} with Equation 5
 - 8: Normalize the deviations d_v to obtain normalized deviations d'_v
 - 9: Compute the score function $\omega(s, a, s') = \lambda \cdot d'_v(s, a, s') + (1 - \lambda) \cdot \hat{A}_{\text{pre}}(s, a, s')$
 - 10: Concatenate \mathcal{D}_{src} and $\{\omega_v\}_{v=1}^{|\mathcal{D}_{\text{src}}|}$ to get $\mathcal{D}'_{\text{src}} = \{(s_v, a_v, r_v, s'_v, \omega_v)\}_{v=1}^{|\mathcal{D}_{\text{src}}|}$
 - 11: **for** $i = 1, 2, \dots$ **do**
 - 12: Sample a mini-batch $b_{\text{src}} := \{(s, a, r, s', w)\}_{v=1}^{N/2}$ from $\mathcal{D}'_{\text{src}}$
 - 13: Sample a mini-batch $b_{\text{tar}} := \{(s, a, r, s')\}_{v=1}^{N/2}$ from \mathcal{D}_{tar}
 - 14: Update the state value function V_ψ via:
 - 15: $\mathcal{L}_V = \mathbb{E}_{(s,a) \sim \mathcal{D}_{\text{src}} \cup \mathcal{D}_{\text{tar}}} [L_2^r(Q_\theta(s, a) - V_\psi(s))]$
 - 16: **// Data filtering**
 - 17: Rank the deviations of the sample source domain data and reject the lowest $\xi\%$ of them
 - 18: Compute the weights for the remaining source domain data by $\exp(\beta\omega'_v)$
 - 19: Compute the target value via: $y = r + \gamma V_\psi(s')$
 - 20: Optimize the state-action value function Q_θ on $b_{\text{src}} \cup b_{\text{tar}}$ via:
 - 21: $\mathcal{L}_Q = \mathbb{E}_{(s,a,r,s') \sim \mathcal{D}_{\text{tar}}} [(Q_\theta(s, a) - y)^2] + \mathbb{E}_{(s,a,d) \sim \mathcal{D}'_{\text{src}}} [\exp(\beta\omega'_v) (Q_\theta(s, a) - y)^2]$
 - 22: Update the target network via: $\theta' \leftarrow \eta\theta + (1 - \eta)\theta'$
 - 23: **// Dataset regularization**
 - 24: Compute the advantage A and optimize the policy π_ϕ on $b_{\text{src}} \cup b_{\text{tar}}$ using advantage-weighted regression (AWR) and dataset regulation:
 - 25: $\mathcal{L}_\pi = \mathbb{E}_{(s,a) \sim \mathcal{D}_{\text{src}} \cup \mathcal{D}_{\text{tar}}} [\exp(\beta A) \log \pi_\phi(a|s) - \beta \cdot \text{KL}(\pi_\phi(\cdot|s) \parallel \pi_{\text{prior}}(\cdot|s))]$
 - 26: **end for**
-

Table 2. Hyperparameter setup for DVDF and baseline methods

Hyperparameter	Value
Shared	
Actor network	(256, 256)
Critic network	(256, 256)
Learning rate	3×10^{-4}
Optimizer	Adam (Kingma, 2014)
Discount factor	0.99
Nonlinearity	ReLU
Target update rate	5×10^{-3}
Source domain Batch size	128
Target domain Batch size	128
IQL	
Temperature coefficient	0.2
Maximum log std	2
Minimum log std	-20
Inverse temperature parameter β	3.0
Expectile parameter τ	0.7
DARA	
Temperature coefficient	0.2
Classifier network	(256, 256)
Reward penalty coefficient λ	0.1
BOSA	
Temperature coefficient	0.2
Maximum log std	2
Minimum log std	-20
Policy regularization coefficient λ_{policy}	0.1
Transition coefficient $\lambda_{\text{transition}}$	0.1
Threshold parameter ρ	$\log(0.01)$
Value weight σ	0.1
CVAE ensemble size of the dynamics model	5
IGDF	
Representation dimension	{16, 64}
Contrastive encoder network	(256, 256)
Encoder pretrained steps	7000
Importance coefficient	1.0
Data selection ratio ξ	25%
OTDF	
CVAE training steps	10000
Number of sampled latent variables M	10
Cost function	cosine
Data filtering ratio ξ	20%
DVDF-IGDF	
SQL pre-training steps	1×10^6
Trade-off coefficient λ	0.7
Data selection ratio ξ	50%
DVDF-OTDF	
SQL pre-training steps	1×10^6
Trade-off coefficient λ	0.7
Data filtering ratio ξ	50%

Table 3. Performance comparison under morphology shifts. half=halfcheetah, hopp=hopper, walk=walker2d, r=random, m=medium, me=medium-expert, mr=medium-replay, e=expert. We report the normalized score evaluated in the target domain, and \pm captures the standard deviation across 5 seeds. We **bold** the highest scores for each task.

Dataset	IQL	BOSA	DARA	IGDF	DVDF-IGDF	OTDF	DVDF-OTDF
half-r	6.7	2.2	2.9	4.9\pm0.3	4.8 \pm 0.1	2.2\pm0.2	2.0 \pm 0.1
half-m	45.8	41.3	45.6	45.5 \pm 0.1	46.0\pm0.3	44.3\pm0.2	42.5 \pm 0.2
half-mr	26.1	27.8	28.9	24.2 \pm 3.3	31.1\pm4.7	19.7 \pm 2.5	27.2\pm1.3
half-me	63.0	44.4	59.2	50.2 \pm 3.4	61.9\pm4.9	42.9 \pm 3.6	53.8\pm4.9
half-e	65.2	78.6	55.4	43.0 \pm 6.2	51.7\pm6.8	74.2 \pm 5.0	91.7\pm7.0
hopp-r	4.7	1.4	4.8	4.8\pm0.2	4.7 \pm 0.1	2.4\pm0.1	1.4 \pm 0.1
hopp-m	56.4	28.7	49.5	55.5\pm2.9	52.7 \pm 4.6	49.1 \pm 2.2	59.4\pm3.7
hopp-mr	51.3	40.6	53.5	54.9 \pm 5.8	58.6\pm6.4	24.9 \pm 3.4	32.6\pm4.5
hopp-me	35.8	20.2	38.2	43.3 \pm 3.6	61.2\pm4.2	51.8 \pm 3.9	63.4\pm5.3
hopp-e	87.2	64.3	77.1	51.5 \pm 2.9	86.9\pm4.2	113.2\pm5.9	109.5 \pm 2.1
walk-r	2.0	1.9	3.9	2.2 \pm 0.1	4.6\pm0.7	0.0 \pm 0.0	0.0 \pm 0.0
walk-m	32.6	40.3	25.0	33.0 \pm 2.3	62.3\pm6.1	40.3 \pm 7.1	61.7\pm9.2
walk-mr	9.0	2.9	6.9	9.5 \pm 0.4	13.6\pm1.2	14.1 \pm 1.8	18.8\pm1.6
walk-me	27.6	46.7	42.2	75.7 \pm 11.8	95.3\pm4.6	66.7 \pm 5.3	73.4\pm6.7
walk-e	103.4	30.2	102.7	108.3\pm6.7	103.5 \pm 5.9	103.5 \pm 1.9	108.8\pm3.2
ant-r	13.6	31.3	26.8	14.4 \pm 1.6	16.0\pm1.7	12.4 \pm 2.2	21.6\pm2.0
ant-m	89.1	36.1	96.4	91.6 \pm 4.4	101.1\pm5.9	92.5 \pm 2.7	102.7\pm3.4
ant-mr	59.7	24.0	64.1	58.2 \pm 7.1	64.8\pm4.6	69.6\pm8.1	57.4 \pm 2.0
ant-me	113.1	100.5	111.9	116.8 \pm 3.5	121.2\pm3.8	107.3 \pm 4.4	120.5\pm2.9
ant-e	116.3	76.3	124.5	126.8 \pm 1.7	129.0\pm2.4	111.0\pm2.4	107.9 \pm 4.0
Total	1008.6	739.7	1019.5	1039.0	1198.7	1042.1	1156.3

Baselines. We maintain the same baselines (IQL, BOSA, DARA, IGDF, and OTDF), and implement DVDF-IGDF and DVDF-OTDF for comparison as in Section 6.1.

Experimental Results. We run each algorithm for 1M gradient steps with 5 random seeds. We present the empirical results under kinematic shifts in Table 5, and the results under morphology shifts in Table 4.

As shown in Table 5, DVDF substantially enhances the performance of base algorithms, elevating total normalized scores by **26.2%** (IGDF) and **27.1%** (OTDF) under kinematic shifts. Specifically, DVDF-IGDF outperforms IGDF in **13** out of 20 tasks, and DVDF-OTDF surpasses OTDF in **12** out of 20 tasks, while achieving comparable performance in the remaining tasks.

The results in Table 4 demonstrate that DVDF maintains superiority over baseline methods under morphology shifts: DVDF-OTDF achieves the highest total score of **373.5** among all methods, surpassing OTDF by **12.6%** and leading in **13** out of 20 tasks. Similarly, DVDF-IGDF improves IGDF by **15.0%** in total score and achieves better performance in **12** out of 20 tasks. These results demonstrate the superiority of DVDF with extremely limited target domain data.

E.3. More Comparisons with Recent Studies

In this section, we compare our method DVDF with two more recent studies, PSEC (Liu et al., 2025) and DmC (Le Pham Van et al., 2025). PSEC proposes to preserve the prior learned skills in a parametric space and adaptively composes them using a context-aware module to handle new tasks. In the cross-domain offline setting, PSEC first learns separate policies from the source domain and target domain data, which are then dynamically combined to work under the target dynamics. DmC employs a KNN-based estimator as a measure of the dynamics gap, and utilizes the KNN proximity score as a guiding signal for diffusion-based data generation. Source domain samples are selected based on the proximity score and combined with the target data for training. As a plug-in method, DVDF could be seamlessly integrated into both PSEC and DmC. Specifically, DVDF could assist PSEC by selecting beneficial source domain samples to facilitate target policy learning from the limited target dataset. Similarly, DVDF could be integrated into DmC’s source data selection process to enable dynamics- and value-aligned data selection. We refer to these two integrated methods as DVDF-PSEC and DVDF-DmC.

Table 4. Performance comparison under morphology shifts with extremely limited target domain data. We report the normalized score evaluated in the target domain, and \pm captures the standard deviation across 5 seeds. We **bold** the highest scores for each task.

Dataset	IQL	BOSA	DARA	IGDF	DVDF-IGDF	OTDF	DVDF-OTDF
half-r	0.0	2.2	2.0	0.0 \pm 0.0	0.0 \pm 0.0	2.0 \pm 0.1	2.2\pm0.1
half-m	18.7	17.3	16.1	22.6 \pm 1.2	26.7\pm3.5	24.6\pm3.4	22.9 \pm 3.6
half-mr	12.5	9.5	8.6	14.8 \pm 1.9	19.4\pm2.0	17.9 \pm 1.6	25.1\pm2.4
half-me	12.3	15.4	13.7	14.9 \pm 0.5	21.9\pm3.1	11.5 \pm 0.8	19.8\pm1.7
half-e	4.9	3.6	2.9	6.2\pm0.1	5.9 \pm 0.2	10.7 \pm 3.5	15.4\pm2.2
hopp-r	3.7	1.1	3.4	4.1\pm0.4	3.8 \pm 0.1	4.4\pm0.2	4.0 \pm 0.1
hopp-m	35.2	20.6	25.5	31.6\pm4.2	20.3 \pm 2.9	24.2\pm3.8	19.3 \pm 2.0
hopp-mr	2.3	3.7	3.5	4.1 \pm 0.3	7.4\pm0.4	4.6 \pm 0.2	5.6\pm0.3
hopp-me	38.3	10.2	19.7	36.3 \pm 3.7	43.2\pm2.8	31.6 \pm 2.9	37.4\pm3.8
hopp-e	28.3	7.3	13.0	29.6 \pm 2.0	44.6\pm7.6	43.3 \pm 6.2	48.9\pm4.1
walk-r	0.0	0.0	0.0	0.0 \pm 0.0	0.0 \pm 0.0	0.0 \pm 0.0	0.0 \pm 0.0
walk-m	16.4	10.6	15.8	14.3 \pm 2.3	24.3\pm1.2	19.3 \pm 2.4	23.7\pm2.2
walk-mr	3.6	0.0	2.9	4.4\pm0.6	3.0 \pm 0.2	4.1 \pm 0.5	4.8\pm0.6
walk-me	16.7	12.8	10.2	12.6 \pm 1.0	20.9\pm3.7	15.4 \pm 1.2	23.0\pm1.5
walk-e	8.3	9.3	12.4	13.9\pm0.1	10.2 \pm 0.4	13.5 \pm 0.4	18.9\pm0.2
ant-r	14.1	20.3	16.2	13.2 \pm 0.4	17.1\pm3.6	10.2\pm0.6	9.1 \pm 0.2
ant-m	17.3	30.1	32.9	25.6 \pm 2.5	28.1\pm5.5	32.3\pm4.0	26.4 \pm 4.4
ant-mr	29.8	19.7	13.5	28.7\pm1.5	19.7 \pm 1.9	20.4 \pm 3.0	27.0\pm2.2
ant-me	15.4	15.8	12.3	17.5 \pm 2.2	21.1\pm2.8	19.1 \pm 1.8	23.2\pm1.9
ant-e	20.7	20.5	23.1	15.8 \pm 1.1	19.0\pm3.2	22.7\pm1.4	16.8 \pm 0.8
Total	298.5	230.0	247.7	310.2	356.6	331.8	373.5

We evaluate DVDF-PSEC and DVDF-DmC on four tasks (halfcheetah, hopper, walker2d, ant) under kinematic shifts, with datasets of three qualities: medium, medium-expert, and expert. All other experimental settings follow Section 6.1. The performance comparison between the base algorithms (PSEC, DmC) and their DVDF-enhanced versions (DVDF-PSEC and DVDF-DmC) is presented in Table 6.

The results in Table 6 show that DVDF-PSEC outperforms PSEC on 11 out of 12 datasets, while DVDF-DmC surpasses DmC on 10 out of 12. Furthermore, the DVDF-enhanced versions achieve a substantially higher total score, confirming the versatility of DVDF as a plug-in module.

F. Compute Infrastructure

We list our compute infrastructure for our experiments in Table 7.

Table 7. Compute Infrastructure

CPU	GPU	Memory
AMD EPYC 7452	RTX3090 \times 8	288GB

G. Training Time

We report the average training time for our method and the baselines (including IQL, IGDF, OTDF, DVDF-IGDF, and DVDF-OTDF) across various tasks over 1M steps in Table 8. Note that the additional computational overhead for OTDF and DVDF stems from solving complex optimal transport matrices and pre-training for the advantage function, respectively. Fortunately, these computations can be precomputed, minimizing their impact on subsequent experiments.

Table 5. Performance comparison under kinematic shifts with extremely limited target domain data. We report the normalized score evaluated in the target domain and \pm captures the standard deviation across 5 seeds. We **bold** the highest scores for each task.

Dataset	IQL	BOSA	DARA	IGDF	DVDF-IGDF	OTDF	DVDF-OTDF
half-r	4.8	2.2	6.7	5.6±1.4	4.8±0.5	2.1±0.1	1.7±0.1
half-m	19.8	23.6	20.4	21.6±0.7	29.7±1.6	22.8±1.9	21.3±2.6
half-mr	5.9	0.0	4.0	7.7±1.2	6.6±2.1	4.0±1.1	9.3±1.5
half-me	9.5	11.1	7.2	14.3±0.9	22.9±1.0	7.6±0.4	13.9±3.7
half-e	7.3	4.2	6.1	4.2±0.1	6.1±0.1	5.2±1.6	4.7±1.0
hopp-r	2.4	1.9	2.2	3.7±0.2	4.2±0.1	1.2±0.1	5.1±1.4
hopp-m	26.1	10.6	13.2	34.6±5.9	38.4±4.1	36.1±4.4	32.8±3.1
hopp-mr	7.4	7.8	9.8	9.8±1.0	13.0±2.9	14.7±3.3	21.3±5.0
hopp-me	9.3	11.4	8.6	12.3±1.4	20.1±5.2	7.1±2.1	15.2±2.9
hopp-e	11.1	8.3	11.8	9.4±0.5	8.0±0.2	6.7±0.3	6.4±0.1
walk-r	4.6	0.0	0.0	8.1±2.9	6.6±1.4	0.0±0.0	0.0±0.0
walk-m	7.7	7.6	4.4	14.3±1.7	23.0±3.9	11.8±1.9	16.1±3.7
walk-mr	3.9	9.1	4.3	2.4±0.1	3.7±0.1	7.4±1.3	16.0±1.6
walk-me	5.7	4.8	6.4	8.4±2.1	16.2±4.4	8.1±2.4	15.9±3.8
walk-e	10.6	9.3	20.1	13.7±2.8	11.9±1.6	15.8±2.0	19.3±1.2
ant-r	7.0	6.5	5.5	11.8±3.0	8.4±2.2	7.3±0.5	10.1±0.6
ant-m	14.6	19.1	21.3	20.3±1.2	24.1±3.3	42.3±7.7	48.1±6.3
ant-mr	7.3	17.6	13.2	3.9±0.7	13.4±2.6	17.6±2.8	14.7±2.3
ant-me	5.3	10.1	2.9	9.4±4.6	9.0±4.8	4.3±0.5	12.3±4.6
ant-e	3.1	4.3	0.0	2.9±1.4	5.5±0.8	5.1±1.2	4.7±1.5
Total	173.4	169.5	141.3	218.4	275.6	227.2	288.9

Table 8. Training time comparison between various methods. h=hour(s), m=minute(s).

IQL	IGDF	OTDF	DVDF-IGDF	DVDF-OTDF
5h24m	6h56m	9h17m	11h43m	14h07m

H. Broader Impacts

This paper presents work whose goal is to promote effective cross-domain offline RL. Our work has potential positive social impacts. For example, our research could enable more efficient development of advanced robotics systems by effectively utilizing source domain data. At present, we have not identified any foreseeable negative impacts arising from this research.

I. LLM Usage Declaration

The use of LLMs in this work is strictly limited to grammatical polishing of the initial draft. LLMs are not involved in any core research components, including but not limited to the conception of the method, theoretical proofs, and experiments.

Table 6. Performance comparison with PSEC and DmC under kinematic shifts. We report the normalized score evaluated in the target domain, and \pm captures the standard deviation across 5 seeds. We **bold** the highest scores for each task.

Dataset	PSEC	DVDF-PSEC	DmC	DVDF-DmC
half-kine-m	33.4\pm1.0	30.1 \pm 0.8	39.6\pm1.1	33.2 \pm 0.2
half-kine-me	41.6 \pm 2.3	49.3\pm2.7	47.3 \pm 5.8	52.6\pm3.2
half-kine-e	52.0 \pm 4.7	58.3\pm3.4	66.9 \pm 2.4	73.6\pm1.6
hopper-kine-m	47.2 \pm 3.5	53.2\pm1.5	53.8 \pm 5.0	65.4\pm2.8
hopper-kine-me	31.7 \pm 3.6	42.0\pm2.4	47.2 \pm 1.3	56.3\pm2.8
hopper-kine-e	70.1 \pm 4.3	74.2\pm3.4	92.6 \pm 2.7	98.2\pm1.6
walker2d-kine-m	41.0 \pm 1.9	56.7\pm5.2	48.3 \pm 4.8	65.1\pm2.4
walker2d-kine-me	53.7 \pm 3.0	58.6\pm3.6	62.6 \pm 2.9	69.2\pm1.2
walker2d-kine-e	75.9 \pm 1.4	95.8\pm2.8	83.0 \pm 2.6	93.0\pm2.6
ant-kine-m	82.2 \pm 1.5	87.4\pm1.4	84.1\pm5.5	81.2 \pm 2.0
ant-kine-me	94.6 \pm 1.7	106.0\pm2.9	107.1 \pm 3.5	112.3\pm2.1
ant-kine-e	103.5 \pm 1.0	118.4\pm1.5	101.2 \pm 1.0	116.1\pm2.9
Total	726.9	830.0	833.7	916.2